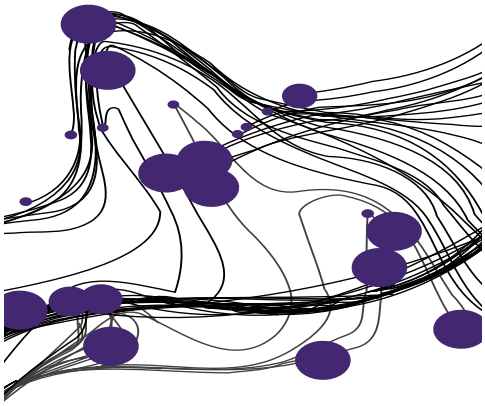

DOSIMETRIC UNCERTAINTY OF LOW-DOSE-RATE PROSTATE BRACHYTHERAPY

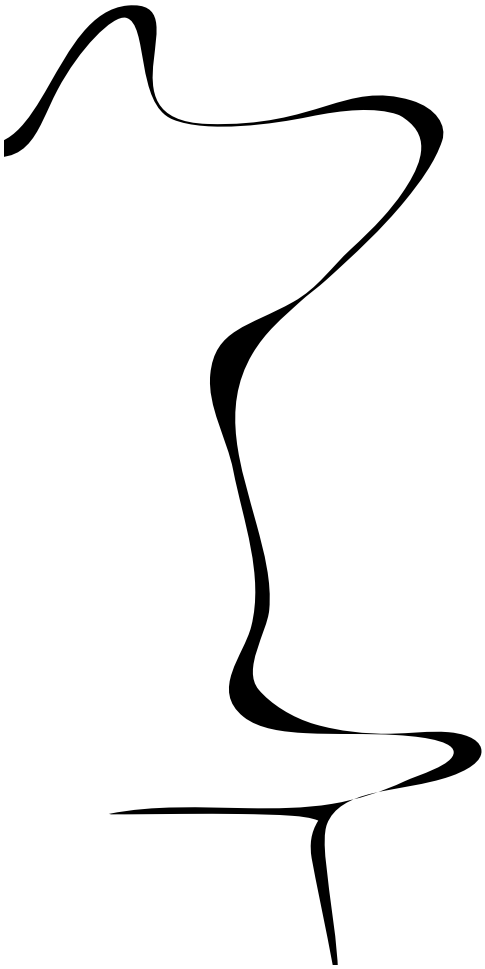

Kathrin Surmann
s1002279

Master Thesis Biomedical Engineering
March 12, 2015

Faculty of Electrical Engineering, Mathematics and Computer Science

Department of Robotics and Mechatronics

In collaboration with

RISO – Radiotherapiegroep, Deventer

EXAMINATION COMMITTEE
Prof. Dr. Ir. C.H. Slump (University of Twente, Enschede)
Ir. H. Westendorp (RISO – Radiotherapiegroep, Deventer)
Prof. Dr. Ir. W. Steenbergen (University of Twente, Enschede)
Dr. J.J. Fütterer (Radboud UMCN, Nijmegen)

DOCUMENT NUMBER
EWI/RAM – 2015-004

UNIVERSITY OF TWENTE.

riso
Radiotherapiegroep

Preface

This thesis is the result of my research performed at the Radiotherapeutisch Instituut Stedendriehoek en Omstreken (RISO, Deventer) and completes my education in Biomedical Engineering at the University of Twente, Enschede.

The presented research would not have been possible without the support and assistance of other people. First of all, I would like to thank Rik Westendorp for his supervision, insight in the different aspects of the LDR procedure and enthusiasm for the profession of the medical physicist. He provided assistance in numerous ways, including the presented analysis and subsequent interpretation of the results. Throughout this project, I appreciated the input and critical feedback of André Minken and Tonnis Nuver. Furthermore, I would like to thank Dinant Kramer who I assisted during some of the source strength measurements.

From the brachytherapy department, I would like to thank Rob Kattevilder for the introduction to the treatment planning system and, together with Ada van der Molen, arranging my visits to the operating theater for observation and research purposes.

Carel Hoekstra, Sandrine van de Pol and Charles Niël introduced me to the clinical part of the procedure. I would like to thank them for their time and expertise.

This master assignment was a collaboration between the RISO and the University of Twente. From the University of Twente, I would like to thank Kees Slump for his supervision and his trust in and appreciation for the applied research performed at RISO. I would also like to thank Jurgen Fütterer and Wiendelt Steenbergen for being members of my examination committee.

Finally, I am grateful for the support and encouragement of my friends and family throughout my bachelor and master, merci, bedankt und vielen Dank.

Kathrin Surmann
Hengelo, February 2015

Abstract

Prostate cancer is the most common type of cancer in males. A well established treatment method is low-dose-rate (LDR) brachytherapy. During LDR brachytherapy, radioactive seeds (e.g. Iodine-125, ^{125}I) are permanently implanted in and around the prostate using transrectal ultrasound (US) guidance. Uncertainties in the procedure include for example target contouring, imaging modalities, treatment planning and source strength. The implementation of LDR brachytherapy differs between institutes and a general list of uncertainties should therefore be tailored to the used procedure. The aim of this project was to (1) investigate and quantify the uncertainties of the LDR procedure as implemented at RISO and (2) suggest improvements to the procedure to possibly reduce these uncertainties.

Uncertainties due to target contouring and multi-modality image registration were assessed in a multi-observer study. Six observers contoured the prostate, urethra and rectum on US and computed tomography (CT) and performed registrations of C-arm conebeam CT (CBCT) with US and magnetic resonance imaging (MRI) for eleven patients. US contouring alone led to a prostate D_{90} variability of 9.3% due to a change in radial distance of 1.1 mm. CT contouring had larger variabilities (D_{90}: 10.3% and 1.9 mm in radial distance) and is not recommended for prostate contouring. Registration variabilities (D_{90}, US–CBCT: 3.1% and MRI–CBCT: 2.1%) were significantly smaller than the contouring variabilities. Manual adjustment of the US–CBCT registrations based on seed and urethra locations was necessary and compensated for the poor fiducial marker visibility on US.

The source strengths of five (separately packaged) ^{125}I seeds are measured for each patient as part of the standard internal quality assurance. The source strength of the patients treated in 2014 varied within 3.0% of the value specified by the manufacturer. This was in agreement with the requirements for LDR brachytherapy sources like ^{125}I.

MRI scans were incorporated in the LDR procedure for seven patients to visualize suspect lesions, the boosts, within the prostate. At the operating theater, previously contoured MRI scans were registered with the pre-implant US scan to transfer the boost structures to the intra-operative US. MRI scans were registered with the post-implant CBCT for the final boost dosimetry. Satisfactory boost dosimetry was achieved for all patients (average V_{150}: 87%, range: 73 - 100). The large pre-implant US slice spacing of 5 mm caused reconstruction artifacts for small boost volumes.

For three patients, the pre-implant US slice spacing was reduced to 2.5 mm, which is equal to the post-implant US scan. Boost volume reconstruction improved.

A combined prostate D_{90} uncertainty of 14% was determined for the LDR procedure as implemented at RISO. The dominant uncertainty of the procedure was target contouring on US (9%). Incorporation of MRI scans for LDR patients with preceding external beam radiotherapy is advised. A smaller pre-implant US slice spacing is recommended for all LDR patients.

Samenvatting

Prostaatkanker is de meest voorkomende kankervorm bij mannen. Low-dose-rate (LDR) brachytherapie is een erkende behandelmethode. Tijdens LDR brachytherapie worden radioactieve zaadjes (bijvoorbeeld jodium-125, ^{125}I) in en rondom de prostaat geplaatst met behulp van transrectale ultrasound (US) geleiding. Bronnen van onzekerheid zijn bijvoorbeeld het intekenen van het doelgebied, de beeldvormende technieken, het plannen van de behandeling en de bronsterkte. LDR brachytherapie wordt in verschillende instituten op verschillende manieren geïmplementeerd en de algemene lijst met onzekerheden moet daarom worden toegespitst voor de gebruikte procedure. Het doel van dit project was (1) het onderzoeken en kwantificeren van de onzekerheden van de LDR procedure bij het RISO en (2) het voorstellen van verbeteringen om deze onzekerheden, indien mogelijk, te verminderen.

Onzekerheden door de intekening van het doelgebied en de registraties van meerdere beeldvormende technieken werden bepaald door middel van een multi-observer studie. Zes observers hebben de prostaat, urethra en het rectum ingetekend op US en computed tomography (CT) en vervolgens registraties van C-arm conebeam CT (CBCT) met US en magnetic resonance imaging (MRI) uitgevoerd voor elf patiënten. De intekening op US leidde tot een prostaat D_{90} onzekerheid van 9.3% door een variatie van de radius van 1.1 mm. Intekenen op CT resulteerde in grotere onzekerheden (D_{90}: 10.3% en 1.9 mm in radius) en wordt niet aanbevolen voor het intekenen van de prostaat. Registratie onzekerheden (D_{90}, US–CBCT: 3.1% en MRI–CBCT: 2.1%) waren aanzienlijk kleiner dan de inteken onzekerheden. Door het handmatig bijstellen van de US–CBCT registraties op basis van de zaadjes en urethra locaties werd de slechte zichtbaarheid van de goudmarkers gecompenseerd.

Als onderdeel van de interne kwaliteitscontrole worden voor elke patiënt de bronsterktes van vijf (apart verpakte) ^{125}I zaadjes gemeten. De bronsterkte varieerde binnen 3.0% van de door de leverancier opgegeven waarde. Dit kwam overeen met de richtlijnen voor LDR brachytherapie bronnen zoals ^{125}I.

MRI scans werden voor zeven patiënten gebruikt tijdens de LDR behandeling om verdachte laesies binnen de prostaat, de boosts, aan te wijzen. Op de operatiekamer werd de van tevoren ingetekende MRI scan geregistreerd met de pre-implantatie US scan om de boost structuren over te zetten naar de intra-operatieve US. Voor de laatste en beslissende dosimetrie werd de MRI scan met de post-implantatie CBCT geregistreerd. Voor alle patiënten werd een toereikende boost dosimetrie gerealiseerd (gemiddelde V_{150}: 87%, gebied: 73 - 100). De grote pre-implantatie US scanafstand van 5 mm veroorzaakte reconstructie artefacten voor kleine boost volumes.

Voor drie patiënten werd deze scanafstand verkleind naar 2.5 mm; de scanafstand van de post-implantatie US. De reconstructie van de boost volumes werd beter.

Een gecombineerde prostaat D_{90} onzekerheid van 14% werd vastgesteld voor de LDR procedure bij het RISO. De dominante onzekerheid van de procedure was de intekening van het

doelgebied op US (9%). Het gebruik van MRI scans wordt geadviseerd voor LDR patiënten met voorafgaande externe bestraling. De verkleinde US scanafstand van 2.5 mm wordt aanbevolen voor alle LDR patiënten.

List of abbreviations

AAPM	American Association for Physicists in Medicine
ABS	American Brachytherapy Society
CBCT	C-arm conebeam computed tomography
CC	Cranio-caudal
CT	Computed tomography
DP	Dosimetric parameter
DVH	Dose-volume-histogram
EBRT	External beam radiotherapy
FM	Fiducial marker
HDR	High-dose-rate
LDR	Low-dose-rate
MRI	Magnetic resonance imaging
NCS	Netherlands Commission on Radiation Dosimetry
NIST	National Institute of Standards and Technology
OR	Operating theater
PA	Posterior-anterior
RISO	Radiotherapeutisch Instituut Stedendriehoek en Omstreken
RL	Right-left
TG-43	Task group 43 of the AAPM
TPS	Treatment planning system
TURP	Transurethral resection of the prostate
US	Ultrasound

Contents

Chapter 1

Introduction

Prostate cancer is the most common type of cancer in males. In Europe, the prostate was estimated as the primary cancer site in 22.8% of the new cases in 2012 [1, 2]. There are several treatment options, including low-dose-rate (LDR) brachytherapy. LDR treatment is chosen for patients with a low to intermediate risk [3] and can be given as monotherapy or in combination with a preceding course of external beam radiotherapy (EBRT) and/or hormonal therapy. For LDR brachytherapy of the prostate, radioactive seeds are permanently implanted in and around the prostate using transrectal ultrasound (US) guidance [4]. The permanent implantation of the seeds demands accurate source placement, imaging and dosimetry. At the Radiotherapeutisch Instituut Stedendriehoek en Omstreken (RISO), US and C-arm cone-beam computed tomography (CBCT) images are registered to combine the visibility of the prostate boundary on US with the excellent seed localization on CBCT [5]. Magnetic resonance imaging (MRI) is considered the gold standard for prostate contouring [4, 6, 7] but is currently not used in the LDR procedure at RISO. The dosimetry at the operating theater (OR) is used to assess the dose given to the target volume as well as the organs at risk. It estimates the quality the implant, ensures proper treatment of the target volumes (i.e. tumor) and minimization of the dose to the healthy tissue.

Uncertainties in the LDR brachytherapy procedure originate from the used technologies as well as the human interaction [8]. Examples for sources of uncertainties are anatomy changes during treatment, imaging technologies, contouring of the regions of interest, treatment planning, and source strength.

In 1987, the first prostate LDR brachytherapy patient was treated at RISO. The intra-operative CBCT was added to the procedure in 2007 and a total of 1240 patients were treated with LDR brachytherapy between 2007 and 2014. It is important to assess the uncertainty of the procedure to ensure proper treatment of the patients and, if necessary, optimize the current procedure. The implementation of LDR brachytherapy differs between institutes [4]. The general list of uncertainties in LDR brachytherapy of Kirisits et al. [8] should therefore be tailored to the used procedure.

In this chapter, some background information is provided together with the research goals and questions. In Chapter 2, 3, 4, 5 and 6, the different sources of uncertainty are explored and assessed. Chapter 7 and 8 focus on the incorporation of MRI scans in the current LDR procedure. Before drawing a conclusion about the dosimetric uncertainties of the LDR procedure at RISO in Chapter 11, the sources and corresponding levels of uncertainty are summarized in Chapter 9 and discussed in Chapter 10. Recommendations for further research and clinical implementations, Chapter 12, complete this thesis.

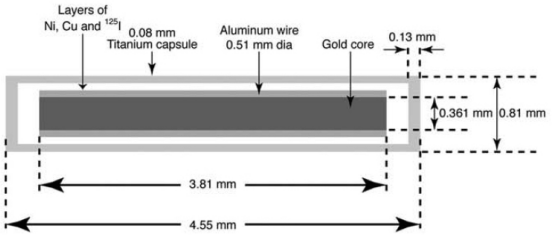

Figure 1.1: STM125I ^{125}I seed used at RISO. [13]

1.1 Background

1.1.1 Brachytherapy

Brachytherapy can be administered with different dose rates. Low-dose-rate brachytherapy has a dose rate of 0.4 - 2.0 Gy/h delivered by permanently implanted radiation sources. The most common radionuclides are iodine-125 (^{125}I) and palladium-103 (^{103}Pd) [3]. In high-dose-rate (HDR) prostate brachytherapy, a high activity source with a dose rate $\geq$ 12 Gy/h (for example iridium-192 or cobalt-60 [9]) is temporarily placed in or around the treatment area [10].

Each radioactive seed has a certain source strength, which is specified in air-kerma strength (S_K) and for convenience reported in U, with 1 U = 1 μGy m^2 h^{-1}. It is defined as the air-kerma rate ($\dot{K}_\delta(d)$, in air, due to photons with an energy larger than δ and at distance d) multiplied by the square distance (d^2) [11, 12]. It accounts for attenuation and scattering of the emitted photons in the air and scattering due to for example the source encapsulation (see Figure 1.1 for a schematic drawing of the ^{125}I seed used at RISO). The American Association for Physicists in Medicine (AAPM) recommends the use the of air-kerma strength as the measure for source strength. However, users and manufacturers often report the source strength as apparent activity (A_{app}), which is defined as "activity of an unfiltered point source of a given radionuclide that has the same air-kerma strength as that of the given encapsulated source" [12]. It does not account for attenuation and scattering of the photons or the interaction with for example the encapsulation. Air-kerma strength can be converted into apparent activity according to the following linear relationship [12]:

$$A_{app} = \frac{S_K}{(\Gamma_\delta)_X} \tag{1.1}$$

$(\Gamma_\delta)_X$ is the exposure rate constant, which is also referred to as the air-kerma conversion factor of 1.27 U/mCi [12]. When reporting the source strength, there is no consensus in the literature. Source strength is given as apparent activity [14, 15, 16], both air-kerma strength and apparent activity [17, 18], or only as air-kerma strength [19, 20, 21]. In the clinically used treatment planning system (TPS), the source strength is entered as apparent activity and converted to air-kerma strength based on the linear relationship of Equation (1.1). In this thesis, it is chosen to report it as apparent activity, since the measurements device for the internal quality assurance assesses the source strength as apparent activity as well.

The TPS calculates the dose for each voxel of a certain structure and summarized them in a dose-volume-histogram (DVH) [22]. From this DVH, the dosimetric parameters (DPs) like V_{100} and D_{90} are determined. V_{100} is the percentage of the structures volume that receives 100%

of the prescribed dose. D_{90} is the percentage of the prescribed dose that 90% of the structures volume receives [23]. Prostate D_{90} and V_{100} are the consensus parameters when reporting the dosimetry of LDR prostate brachytherapy.

The dose calculation is based on an established formalism introduced by the Task Group 43 of the AAPM [11, 12]. It describes the dosimetry of brachytherapy sources and is referred to as TG-43 formalism. The exact implementation and choice of parameters is dependent on the TPS.

1.1.2 LDR procedure at RISO

For LDR treatment, ^{125}I seeds are permanently implanted in the prostate through the perineum (see Figure 1.2), causing trauma and swelling of the prostate and the surrounding tissue. The prescribed dose is 145 Gy for LDR monotherapy and 100 Gy for LDR treatment with preceding EBRT. For all LDR brachytherapy patients, an US volume study is performed for preplanning and ordering of the seeds. When patients receive the combination of EBRT and LDR treatment, MRI scans are acquired as well. The MRI scans (T1- and T2-weighted) are used for target definition during EBRT planning. If LDR brachytherapy is combined with EBRT, four gold fiducial markers (FMs) (Heraeus GmbH, Hanau, Germany) are implanted before starting EBRT. The FMs are used for position verification and patient alignment during EBRT. For patients with LDR monotherapy, these FMs are implanted at the operating theater just before seed implantation. During the LDR part of the treatment, the rigid registration of US and (CB)CT is initiated with the localization of the FMs. Coordinates are defined according to the Dicom coordinate system in Figure 1.3. At the OR, the needles are guided by US and their location and penetration are verified by fluoroscopy [5]. For the final dosimetry at the OR, the post-implant US is registered with a CBCT based on rigid transformation to minimize the residual distance between the FMs localized on both modalities. The registration can be manually adjusted based on urethra and ^{125}I seed locations if necessary. A detailed description of the LDR procedure, after preceding EBRT, at RISO can be found in Figure 1.4. At Day 30, another CT scan is made and registered with the pre-implant US from the OR. The dosimetry is assessed. A new CT scan is acquired because the implant and surrounding tissues underwent changes between the implantation procedure and the Day 30 dosimetry check. Seeds can have migrated or been excreted [14, 15, 24]. The pre-implant US is used because the edema due to trauma from needle insertion is mostly resolved at Day 30 [16, 25].

1.1.3 Uncertainties

An uncertainty is defined as a "parameter, associated with the result of a measurement, that characterizes the dispersion of values that could reasonably be attributed to the measurand" [27]. Uncertainties can be quantified and are generally reported as standard deviations, whereas accuracy is qualitative [27].

For each source of uncertainty, a level of uncertainty is quantified in the following chapters. The combined standard uncertainty (u_c) is defined in Equation (1.2) [8, 27, 28]:

$$u_c = \sqrt{\sum_{j=1}^{J} {u_j}^2} \tag{1.2}$$

J is the number of sources of uncertainty and u_j is their respective standard uncertainty. It is assumed that the uncertainties are independent of each other.

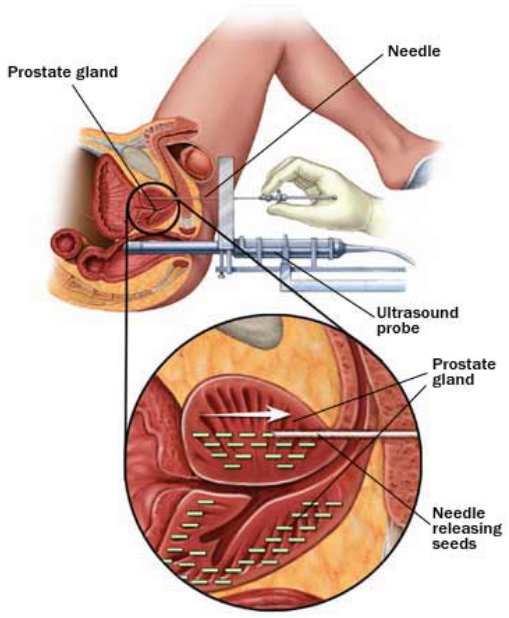

Figure 1.2: Implantation of seeds in the prostate under transrectal US guidance. [26]

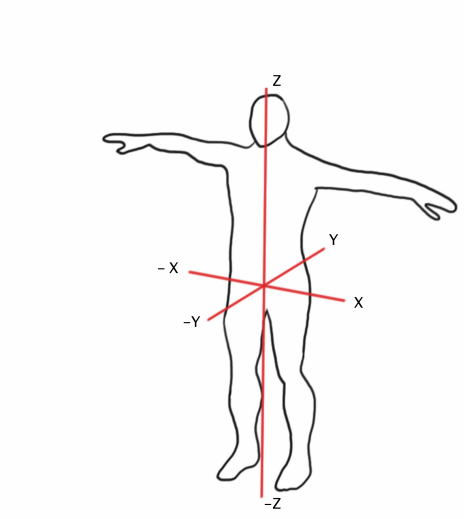

Figure 1.3: Coordinate system as defined in Dicom with x-y as transversal plane, y-z as sagittal plane and x-z as coronal plane.

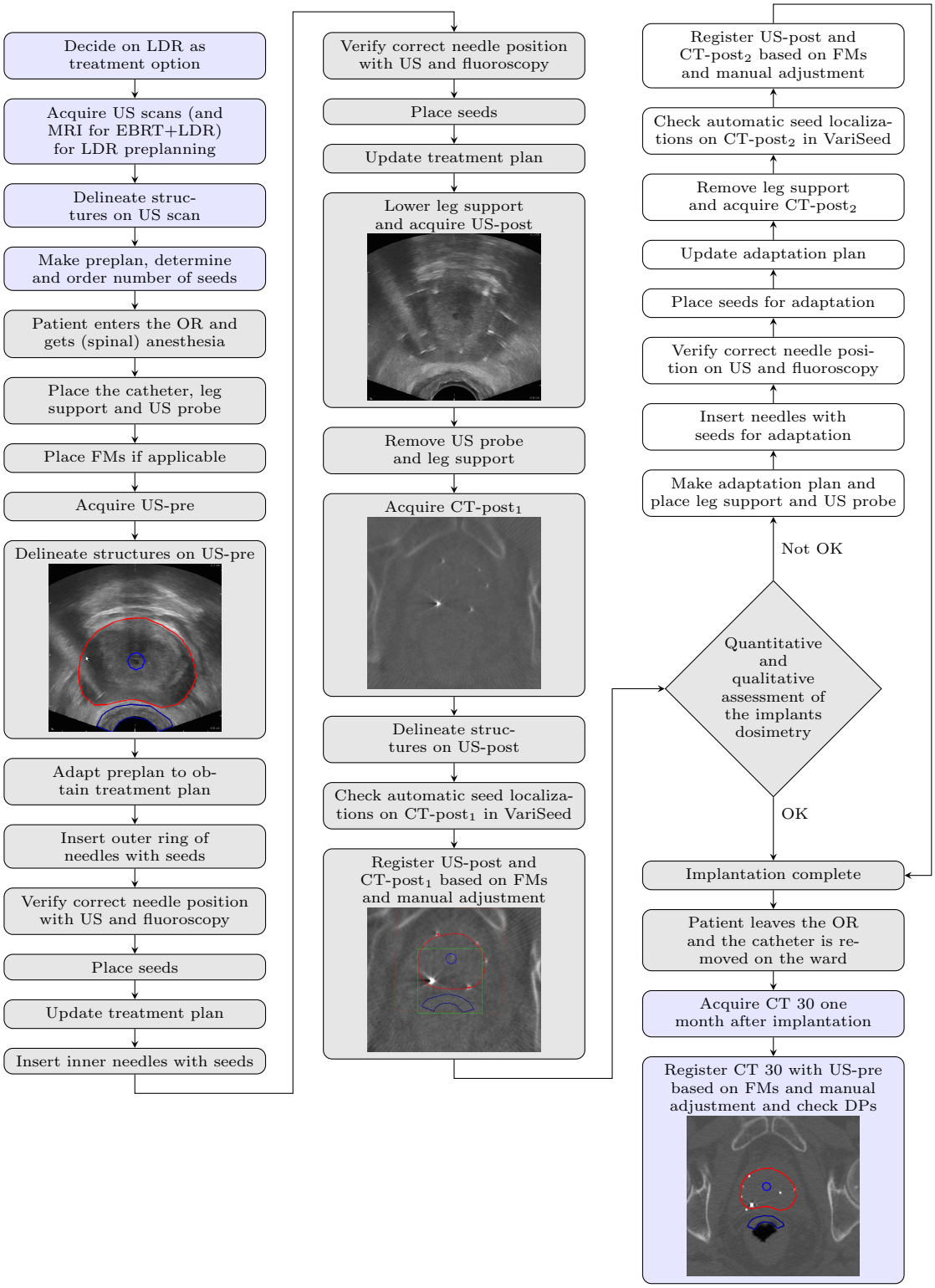

Figure 1.4: Work flow for the LDR brachytherapy procedure of the prostate with ^{125}I seeds at RISO. The blue steps are performed outside the OR before or after the implantation procedure. All gray steps are part of the standard procedure at the OR. White steps are carried out if the implant needs adaptation at the OR.

1.2 Research goal and questions

The *aim* of this study is to investigate uncertainties in the LDR brachytherapy procedure of the prostate as implemented at RISO. The effect of these uncertainties on the dosimetry is quantified by experiments, simulations, and literature research. Improvements to the current LDR brachytherapy procedure are proposed and, if possible, implemented.

In order to accomplish these *research goals*, a set of *research questions* has to be answered.

A multi-observer study is designed to assess the dosimetric consequences of inter- and intra-observer contouring and registration. In Chapter 2, the following questions are answered:

- *What is the geometric and dosimetric uncertainty of inter- and intra-observer contouring on US and CT?*
- *What is the uncertainty of the current rigid US–CBCT registration based on FMs and manual adjustment?*
- *What uncertainty is introduced by MRI–CBCT registration?*

^{125}I seeds are delivered in batches with a specified apparent activity. Quality assurance at our institute is performed to verify the apparent activity before the implantation procedure. These measurements are presented in Chapter 3:

- *What is the deviation between the specified and measured apparent activity of the ^{125}I seeds?*

The implementation of the TG-43 formalism is reviewed in Chapter 4:

- *What is the uncertainty introduced by the implementation of the TG-43 formalism in the clinically used treatment planning system?*
- *How does the target medium affect the dosimetry?*
- *What is the dosimetric consequence of the interaction between emitted photons and the implanted ^{125}I seeds?*

Uncertainties due to treatment delivery imaging are explored in Chapter 5:

- *What is the dosimetric uncertainty of seed localization on CT?*
- *What is the uncertainty introduced by the dose matrix resolution in the clinically used treatment planning system?*

Changes of the implant between the implantation procedure and post-implant imaging are investigated in Chapter 6:

- *How does seed migration and loss affect dosimetry?*
- *What is the dosimetric uncertainty when accounting for edema?*

MRI scans can be used in the LDR procedure to visualize structures within the prostate that are not visible on US and (CB)CT scans. In Chapter 7, feasibility and dosimetry are explored:

- *Is it possible to incorporate MRI scans in the current LDR procedure?*
- *What dose level is achieved in the suspect lesions?*

In Chapter 8, a method is tested to improve the boost dosimetry and geometry:

- *Will a decreased pre-implant US slice spacing improve boost volume reconstruction after US–MRI registration?*

Part I

Sources of uncertainty:

Experiments and simulations

Chapter 2

Inter- and intra-observer contouring and multi-modality image registration

2.1 Introduction

Different imaging techniques can be used during LDR brachytherapy, including US, (CB)CT and MRI [4]. MRI is considered the gold standard for prostate contouring due to its high soft-tissue contrast. It shows superior contouring reproducibility and better correspondence with US compared to CT [6, 7]. The prostate can be accurately visualized with US, whereas the seeds and FMs are less visible on US. Previous phantom studies at RISO suggested the use of another FM to enhance visibility on US and MRI [29, 30]. Seeds and FMs are clearly visible on CT. However, CT has low soft-tissue contrast leading to relatively low accuracy and reproducibility of contoured structures, compared to US and MRI [7].

At our institute, US and CBCT scans are registered for dose assessment to combine the visibility of the prostate boundary on US with the accurate seed localization on CT [5, 16]. The rigid registration is started based on four FMs and then manually adjusted if necessary. Multi-modality image registration and prostate contouring have been shown to introduce uncertainties in the procedure that affect dosimetry results [6, 8, 31]. Post-implant dosimetry is of importance for quality assurance of the LDR procedure and is predictive for clinical outcome [32, 33].

The inter-observer variability of the prostate DPs has been investigated in a study including observers from six different European institutes [6]. Five to seven observers participated in the different parts of a contouring, seed localization and image fusion study with three patients. Other studies were performed to examine the geometrical differences in prostate contouring between observers in radial distances [34, 35] or volumes [7]. Contouring depends on personal as well as institutional definitions and habits [6, 7] and dosimetric differences of one study cannot be directly compared with or translated to geometrical differences of another study. To our knowledge, there has not been a single study including both.

In this chapter, the variabilities in post-implant dosimetry at RISO are investigated. The dosimetric inter- and intra-observer variabilities of US– and MRI–CBCT registrations are quantified. Both geometrical and dosimetric variabilities due to US and CT contouring are investigated.

2.2 Materials and methods

2.2.1 Patients

Eleven patients (five T1c, four T2b, one T2c and one T3b) were treated with a LDR boost with ^{125}I seeds after EBRT between January and August of 2013. Each patient received 47 Gy (20×2.35 Gy) with EBRT and 110 Gy with brachytherapy. Additional information can be found in Appendix A.1 Table A.1.

2.2.2 Image acquisition

T1- and T2-weighted MRI scans (T1 and T2) were made on average 55 days (range: 47 - 62) prior to LDR brachytherapy with a 3T MRI scanner (Signa HDxt; GE Medical, Milwaukee, WI, USA) and a slice spacing of 2 mm. The US scans obtained directly before and after ^{125}I seed implantation (US-pre and US-post) were acquired with a FlexFocus 400 US system (BK Medical, Herlev, Denmark) and an increment of 5 and 2.5 mm, respectively. A CBCT (Siemens Arcadis Orbic 3D; Siemens Medical Systems, Erlangen, Germany) was used to generate CT-post directly after seed implantation with a slice spacing of 2.5 mm. The registration of CT-post and US-post was used for post-implant dosimetry at the operating theater. On average 31 days (range: 27 - 38) after implantation, CT 30 was acquired with a conventional CT scanner (Brilliance Big Bore 16 Slice; Philips, Best, The Netherlands) to assess the Day 30 dose distribution. The slice spacing was 2 mm.

2.2.3 Multi-observer study

Six observers from our institute contoured structures, selected FMs and registered images three times for eleven patients. To prevent bias, the three sessions were performed at least one week apart. The observers were the three very experienced radiation oncologists that routinely perform the LDR procedure (obs 1 - 3), the author (obs 4), a medical physicist who is experienced in the LDR procedure (obs 5) and a dedicated research brachytherapy technologist (obs 6). Observer 4 had no previous experience in prostate contouring or registration and received explanations and instructions from observer 1 for the purpose of performing this study. Observer 3 completed only the first session. The detailed instructions for the three sessions can be found in Appendix A.2 and A.3.

The multi-observer study was performed in the clinically used TPS, VariSeed (Version 8.0; Varian Medical Systems Inc., Palo Alto, CA, USA). The obtained studies were exported as Dicom files and further processed in Matlab (Version 8.1.0.604; The MathWorks Inc., Natick, MA, USA). The statistical analysis was performed in SPSS (Version 22.0.0.0; International Business Machines Corporation, Armonk, NY, USA).

The observers contoured the prostate, urethra and rectum on US-pre three times and the prostate and rectum once on CT 30. During the acquisition of CT 30, there was no catheter used and the urethra was therefore not visible. CT contouring was performed only once due to the poor soft-tissue contrast, even taking into account to superior soft-tissue contrast of a conventional CT scan compared to a CBCT scan.

The centers of the four FMs were selected on US-post three times, and once on CT-post and T1. T1 was chosen due to its superior FM visibility compared to T2. US-post and CT-post were chosen since these scans were used for dosimetry during the implantation procedure. Anatomical locations (e.g. cranial left or caudal left) of FMs that could not be found on US

due to bad visibility were noted. The data sheets of the multi-observer study can be found in Appendix A.4.

Registrations of US– and MRI–CBCT were performed three times as well. The observers were instructed to use the four FMs to start the rigid transformation in VariSeed. The registration could then be manually adjusted with translation and/or rotation before the calculation of the DPs. Again, the locations of FMs not found or not used during the registration process were noted. To perform a 3D transformation, only three of the four FMs were necessary.

The following DPs were obtained after each registration:

- Prostate V_{100} ($\geq$ 98%)
- Prostate D_{90} (100–110%)
- Urethra D_{30} ($<$ 125%)
- Rectum V_{100} ($<$ 1 cm^3)

The accepted ranges for post-implant dosimetry at the OR are given in the brackets. V_{100} describes the percentage of the prostate volume that receives 100% of the prescribed brachytherapy dose. D_{90} describes the percentage of the prescribed brachytherapy dose that 90% of the prostate volume receives [23].

2.2.4 Processing and analysis

Reference data sets

All contours and DPs were compared with the clinically used data set, which consists of the contours on US-pre, the seed distribution on CT-post and the contours on CT 30 obtained at the Day 30 dosimetry check by the registration of US-pre and CT 30. DPs were compared with the DPs obtained from the registration at the OR and the Day 30 dosimetry. The clinical data set was considered as ground truth and used for comparison.

FMs were not localized in the clinical data set and the distances were calculated with respect to the average position of all observations.

MRI scans are currently not used for the clinical LDR procedure. For the purpose of this study, the prostate and rectum were contoured on T2 and transferred to T1 by an experienced radiation oncologist, observer 1, for the dosimetry after MRI–CBCT registration.

Contouring

The contours obtained from each observer were processed and analyzed with a Matlab script. After linear interpolation between the contour points imported from VariSeed, the prostate contour was translated and rotated to place the center of the prostate in the origin of the coordinate system. A detailed description can be found in Appendix A.5. Sample points of the prostate were then taken at 10° increments of the polar and azimuthal angles [7] (see Figure 2.1a). The Euclidean distance of the center of the urethra localized by the observer and derived from the clinical data was calculated per slice (see Figure 2.1b). The rectum was resampled per slice with the center of the US probe as origin. After linear interpolation between the contour points imported from VariSeed, samples were taken at 10° intervals (see Figure 2.1c).

Each structure was divided into three equal parts: cranial, central and caudal. This division was made based on the craniocaudal length of the prostate in the clinical data set (see Figure 2.2). Only the parts of the urethra and rectum close to or within the prostate, i.e. contoured on slices that contain prostate contours, were considered in the analysis since they are affected by dose

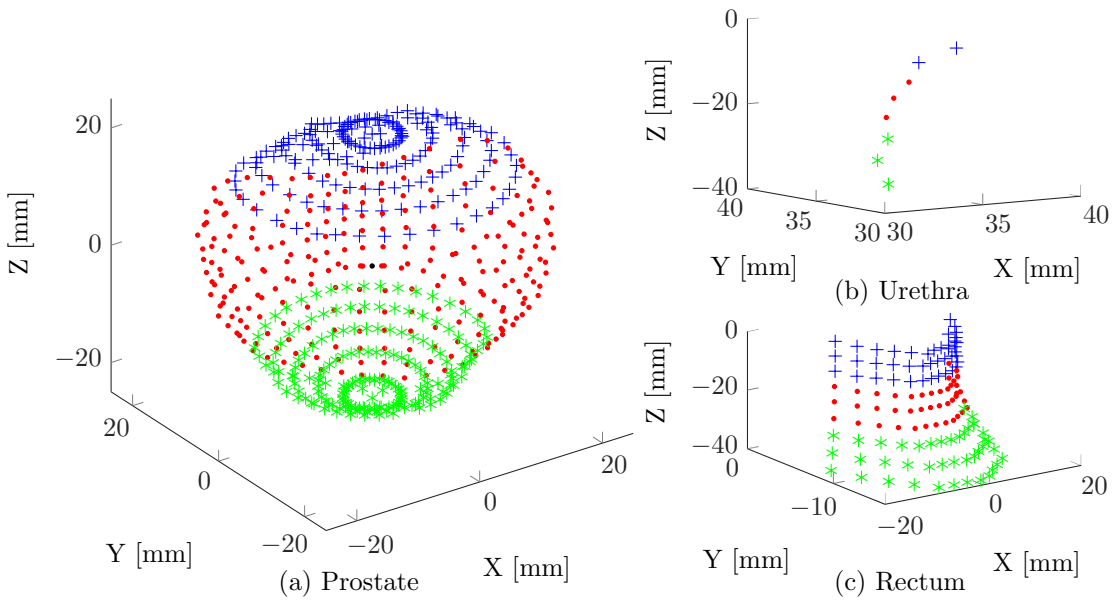

Figure 2.1: Sample points of the clinical contours of the (a) prostate, (b) urethra and (c) rectum of patient 3 on US. Sample points of the prostate were taken at each 10° × 10° solid angle from the center of mass. The urethra was sampled at the center of each slice. Sample points of the rectum were taken in each slice at each 10° between -155° − -25°. Each structure was divided into cranial (+), central (●) and caudal (∗) parts based on the craniocaudal length of the prostate.

distribution and possible complication.

The clinically used contours in the Day 30 dosimetry were replaced by the observer contours to investigate the variability of the DPs based on contouring alone. In VariSeed, the scan contoured by the observer was imported and the contours were replaced.

To remove natural variation in DPs between patients, the DPs were normalized with the patient's clinical DP (for the inter-observer variability) or the average DP after the three sessions per observer and patient (for the intra-observer variability). The standard deviation is then calculated according to Equation (2.1) as inter-observer variability or according to Equation (2.2) as intra-observer variability.

$$SD_{clin} = \sqrt{\frac{1}{POS}\sum_{p=1}^{P}\sum_{o=1}^{O}\sum_{s=1}^{S}\left(\frac{X_{p,o,s}}{C_p} - \overline{C}\right)^2}, \quad \textit{with } \overline{C} = 1 \textit{ due to normalization} \tag{2.1}$$

$$SD_{obs} = \sqrt{\frac{1}{POS}\sum_{p=1}^{P}\sum_{o=1}^{O}\sum_{s=1}^{S}\left(\frac{X_{p,o,s}}{\frac{1}{S}\sum_{s=1}^{S} X_{p,o,s}} - \overline{X}\right)^2},$$

$$\textit{with } \overline{X} = \frac{1}{POS}\sum_{p=1}^{P}\sum_{o=1}^{O}\sum_{s=1}^{S}\frac{X_{p,o,s}}{\frac{1}{S}\sum_{s=1}^{S} X_{p,o,s}} \tag{2.2}$$

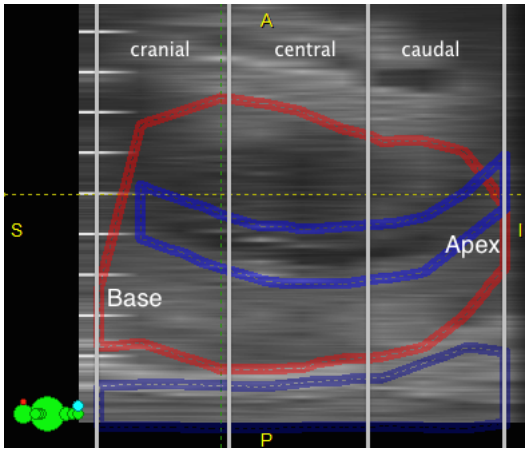

Figure 2.2: Cranial, central and caudal sections of the structures of interest. Sagittal view of US-pre of patient 1 in VariSeed with the clinically used contours: prostate (red), urethra (blue) and rectum (purple).
A = anterior; P = posterior; S = superior; I = inferior.

P is the number of patients, O the number of observers and S the session. $X_{p,o,s}$ described the DP obtained for patient p by observer o during session s. C_p denotes the clinical DP of patient p of the respective study, US or CT. For rectum V_{100}, the values are given in cm^3 instead of percentage of prescribed dose. Normalizing it would not lead to representative variabilities due to the small volumes (often 0 - 1 cm^3). The rectum is not contoured on US-post and clinical DPs are available for only one patient. The observed rectum V_{100} was subtracted by the average V_{100} of all observations per patient (inter) or the average of the three sessions per patient and observer (intra). The resulting SD_{clin} and SD_{obs} were then the absolute difference and not a percentage of the used reference.

The respective DPs of US and CT contouring were tested for statistical significance with an independent-sample t-test and a 95% level of confidence.

When calculating the geometrical variabilities, the distance between the patients clinical contours (inter) or average of the three contouring sessions (intra) and the observer contours was calculated per sample point. This was averaged per structure or part before calculating $SD_{clin,mm}$ and $SD_{obs,mm}$ according to Equation (2.3).

$$SD_{mm} = \sqrt{\frac{1}{POS}\sum_{p=1}^{P}\sum_{o=1}^{O}\sum_{s=1}^{S}\left(D_{p,o,s} - \overline{D}\right)^2}, \quad with\ \overline{D} = \frac{1}{POS}\sum_{p=1}^{P}\sum_{o=1}^{O}\sum_{s=1}^{S} D_{p,o,s} \tag{2.3}$$

$D_{p,o,s}$ described the average difference for patient p contoured by observer o during session s. For the inter-observer variability, it was calculated as

$$D_{p,o,s} = \frac{1}{N}\sum_{n=1}^{N}\left(RO_{p,o,s,n} - RC_{p,n}\right), \tag{2.4}$$

with $RO_{p,o,s,n}$ as observer distances and $RC_{p,n}$ as distance of the clinical contours. N is the number of sample points of the investigated structure.

For the intra-observer variability, it was calculated as

$$D_{p,o,s} = \frac{1}{N}\sum_{n=1}^{N}\left(RO_{p,o,s,n} - \frac{1}{S}\sum_{s=1}^{S} RO_{p,o,s,n}\right). \tag{2.5}$$

Registration

Localization of the FMs on US is difficult due to their poor visibility. FMs with an Euclidean distance to the mean FM position $\geq$ 3 mm were assumed to be falsely localized [9] and were removed from the data set. This outlier removal was also applied to the FMs localized on CBCT and MRI. The variabilities in FM localization were determined with Equation (2.3). There were no clinical localizations for comparison, so the average location of all observations per FM was chosen as reference.

For each registration, DPs were retrieved from VariSeed and inter- and intra-observer variabilities were calculated as SD_{clin} and SD_{obs} respectively, similar to the dosimetric variabilities of US and CT contouring (see Equation (2.1) and (2.2)). The respective DPs of US– and MRI–CBCT registrations were tested for statistical significance with an independent-sample t-test and a 95% level of confidence.

2.3 Results

2.3.1 Contouring

Inter-observer variability (1 SD with respect to the clinically used contours) for the whole prostate on US was 1.1 mm and 2.1, 0.4 and 2.0 mm for the cranial, central and caudal parts respectively. When only the experienced observers are considered, this reduced to 0.8, 1.9, 0.3 and 1.4 mm respectively. The intra-observer variability (1 SD with respect to the average of the three observer contours) was 0.6 mm for the whole structure and 0.9, 0.4 and 1.0 mm for cranial, central and caudal parts, respectively. This was 0.5, 0.8, 0.3 and 0.6 mm for only the experienced observers. When comparing the experienced with the inexperienced observers, significant differences were found for the caudal part ($p < 0.01$) while the differences of the whole prostate and the central part were almost significant ($p = 0.05$ and $p = 0.05$). The cranial part did not have significant differences between experienced and inexperienced observers ($p = 0.62$).

Contouring on CT resulted in an inter-observer variability of 1.9 mm for the whole structure and 3.0, 2.3 and 3.6 mm for the cranial, central and caudal parts, respectively. The experienced observers alone had an inter-observer variability of 1.4 mm for the whole prostate and 2.2, 1.4 and 3.6 mm for the respective parts. The large difference with the clinical contours of up to 5.1 mm, averaged over the whole prostate, gave enough indication to not further investigate the CT contouring variabilities. In addition, observers mentioned that their prostate contour was partly based on the ^{125}I seeds.

The differences resulting from all contouring performed during the multi-observer study are displayed in Figure 2.3 and 2.4. For one patient, observer 5 localized a calcification instead of the urethra during session 1 and 2. These contours and the respective DPs were excluded from the analysis. The observers contoured the prostate smaller than the clinically used contours, especially in the cranial and caudal parts (see Figure 2.3). The cranial and caudal parts had larger inter- and intra-observer variabilities than the central part on US as well as on CT.

Observer contours were also used for dosimetry. The results can be seen in Figure 2.5 and Table 2.1. Prostate contouring on CT showed significantly (for both DPs $p < 0.01$) larger inter-

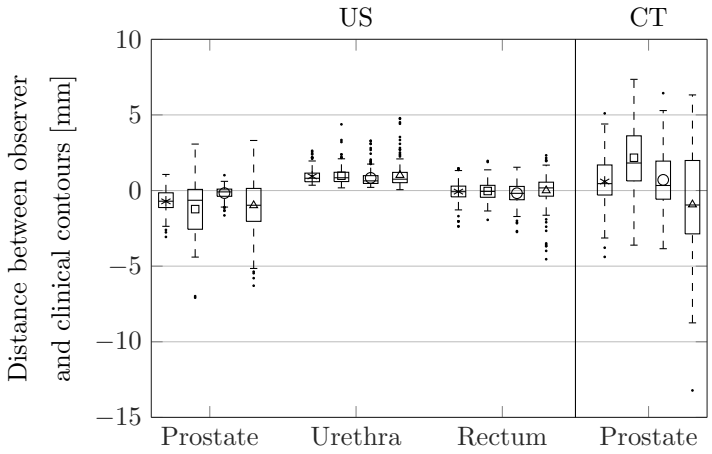

Figure 2.3: Distance between the observer and clinical contours for the whole structure (∗) and cranial (□), central (○) and caudal (△) parts of the prostate, urethra and rectum on US and the prostate on CT. The symbol is depicted at the mean.
Contouring on CT took place once whereas US contouring was performed three times.

observer variabilities (5.5% for V_{100} and 10.3% for D_{90}) than on US (1.6% for V_{100} and 9.3% for D_{90}). Furthermore, the dosimetric intra-observer variability due to US contouring was smaller than the inter-observer variability (see Table 2.1). The prostate was contoured smaller on US and larger on CT, leading to respectively larger and smaller D_{90}'s than for the clinical contours.

2.3.2 Registration

During FM localization, observers found 83.5% of the FMs on US and 100% on CBCT and MRI. Outlier removal showed that 68.2% of the FMs on US were within 3 mm of the mean FM position and therefore considered correctly localized. 99.6% of the FMs on CBCT were included and 95.2% on MRI. When examining the FMs noted as "not found" during the registrations, observers found 91.3% of the FMs on US, 100% on CBCT and 99.3% on MRI.

After outlier removal, inter-observer variabilities of FM localization were comparable between US, CBCT and MRI with Euclidean distances of 1.3, 1.2 and 1.5 mm (1 SD with respect to the mean FM position) respectively. Distances in the right–left (RL) and posterior–anterior (PA) direction were comparable as well; 0.4, 0.3 and 0.3 mm in RL and 0.5, 0.3 and 0.4 mm in PA. The cranio–caudal (CC) distances were larger for all three modalities (1.1, 1.1 and 1.4 mm respectively). The intra-observer variabilities on US (0.3 mm in RL and PA direction, 0.9 mm in CC direction and 1.0 mm Euclidean distance) were smaller than the inter-observer variabilities. For patient 6, sharp reflections of the seeds led to false localizations and he was excluded from the analysis of FM variability on US. For patients 2 and 3, there were no MRI scans available. During visual verification of the zero-match of T1 and T2, patient 10 showed different reference coordinates for T1 and T2. These three patients were not included in the MR part of the multi-observer study.

US–CBCT registration was manually adjusted by translation and/or rotation in 78.4% of the studies. 17.6% of all MRI–CBCT registrations were manipulated after the rigid transformation based on FMs.

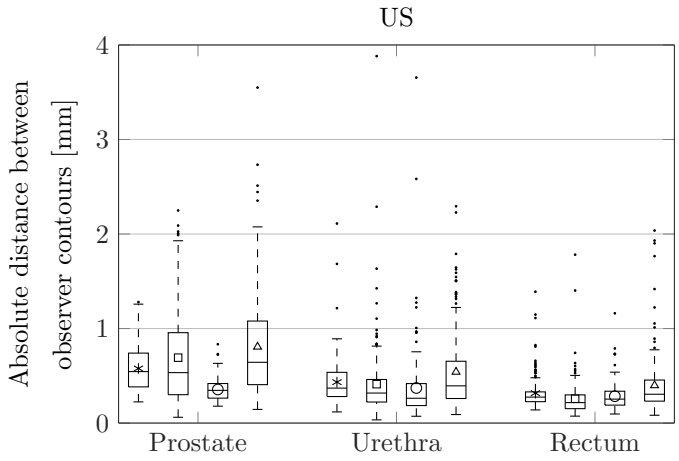

Figure 2.4: Absolute distances between the three repeated contours of each observer for the whole structure ($*$) and cranial ($\square$), central ($\bigcirc$) and caudal ($\triangle$) parts of the prostate, urethra and rectum on US. The symbol is depicted at the mean.

Dosimetric results of the registrations are shown in Figure 2.5 and 2.6. The corresponding inter- and intra-observer variabilities can be found in Table 2.1, together with the clinical mean and the average normalized DPs. MRI–CBCT registrations had significantly smaller inter-observer variabilities than US–CBCT registrations for prostate V_{100} ($p < 0.01$) and D_{90} ($p = 0.04$). D_{90} variabilities were generally larger than V_{100} variabilities due to the upward restriction of $V_{100} \leq 100\%$; the so-called clipping. When testing the intra-observer US– and MRI–CBCT registrations, both V_{100} ($p = 1$) and D_{90} ($p = 1$) showed no significant difference.

2.4 Discussion

2.4.1 Contouring

During our study, the largest variabilities were found in the cranial and caudal sections of the prostate (see Figure 2.3 and 2.4). These are the most uncertain regions when contouring the prostate. There was no significant difference between experienced and inexperienced observers, indicating the difficulty even for experienced radiation oncologists. Smith et al. [7] reported geometrical inter-observer variabilities of up to 2.2 mm in the anterior and posterior regions of the cranial part of the prostate on CT. Their study was performed with seven observers and two iterations. They found comparable variabilities in 3D transrectal US and CT contouring. In our study, US contouring was closer to the clinical data set than CT contouring and showed a smaller variation in geometrical differences (Figure 2.3) as well as significantly smaller variations in dosimetric parameters (see Figure 2.5 and SD_{clin} in Table 2.1). Observers mentioned that their prostate contouring on CT scans was partly based on the visible ^{125}I seeds due to the lacking visibility of the prostate boundary.

Urethra contouring on US was more accurate than prostate contouring (see Figure 2.3 and 2.4) due to the distinctive front and back reflection of the urinary catheter. The cranial part with the Foley balloon and the caudal part where the urethra exits the prostate showed larger variabilities. The rectum was also accurately contoured. The variability increased from cranial

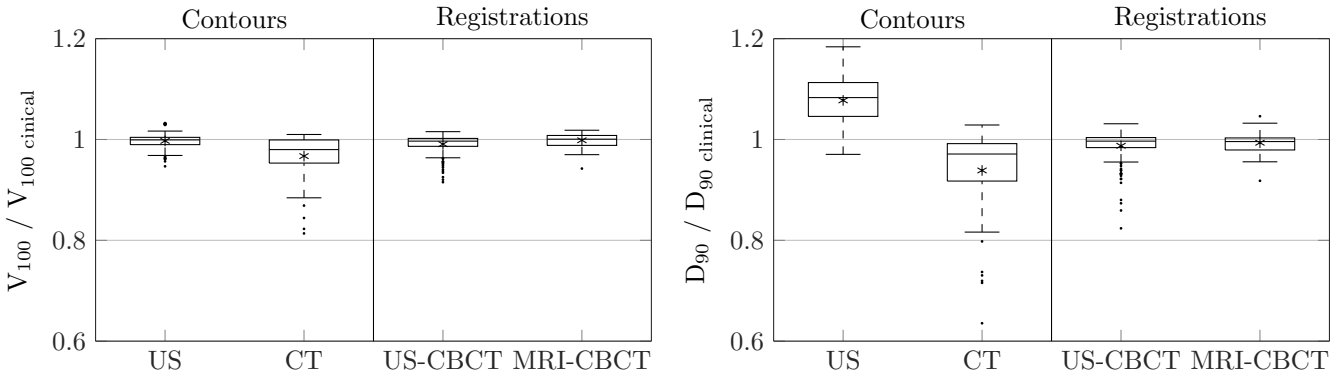

Figure 2.5: Prostate V_{100} (left) and D_{90} (right), normalized with the respective clinical DP, originating from observer contours on US and CT and registrations of US– and MRI–CBCT. The symbol ($*$) is displayed at the mean.
Contouring on CT took place once whereas US–CBCT and MRI–CBCT registration and US contouring were performed three times.

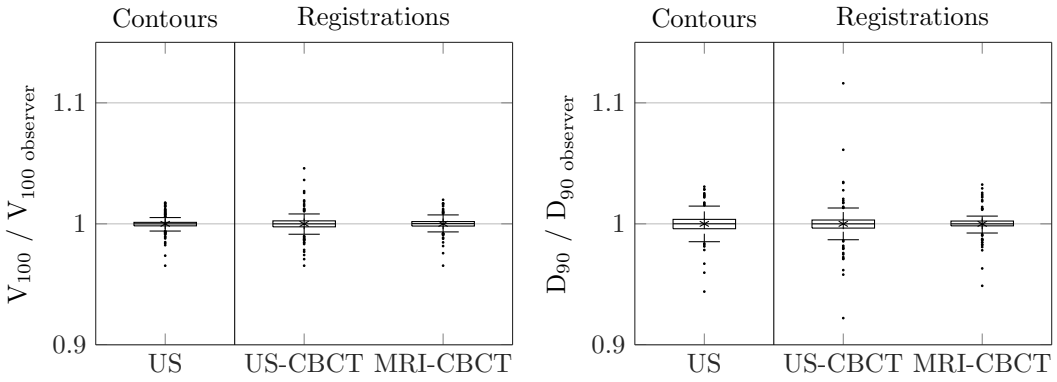

Figure 2.6: Prostate V_{100} (left) and D_{90} (right), normalized with the average observer DP of the three sessions, originating from observer contours on US and registrations of US– and MRI–CBCT. The symbol ($*$) is displayed at the mean.

Table 2.1: Inter- and intra-observer variability of the dosimetric parameters (DPs) based on US and CT contours and US– and MRI–CBCT registration. Average clinical DPs and scaled observer DPs are given. SD_{clin} (1 SD with respect to the clinical average) describes the inter-observer variability, whereas SD_{obs} (1 SD with respect to the observer average) describes the intra-observer variability.

	US cont.	CT cont.	US–CBCT	MRI–CBCT
Prostate V_{100}				
Clinical mean [%]	98.8	98.8	98.4	98.2
Average Observer/Clinical	1.0	1.0	1.0	1.0
SD_{clin}[%]	1.6	5.5	2.0	1.3
SD_{obs}[%]	0.6	–	0.9	0.7
Prostate D_{90}				
Clinical mean [%]	122.1	122.1	113.5	114.2
Average Observer/Clinical	1.1	0.9	1.0	1.0
SD_{clin}[%]	9.3	10.3	3.1	2.1
SD_{obs}[%]	1.0	–	1.5	1.0
Urethra D_{30}				
Clinical mean [%]	136.4	–	119.6	–
Average Observer/Clinical	1.1	–	1.0	–
SD_{clin}[%]	14.6	–	2.4	–
SD_{obs}[%]	1.4	–	1.6	–
Rectum V_{100}				
Clinical mean [cm^3]	0.8	0.8	–	–
Observer mean [cm^3]	2.3	1.0	–	1.2
SD_{clin}[cm^3]	0.4	0.5	–	0.6
SD_{obs}[cm^3]	0.2	–	–	0.5

– Not available.

to caudal as the distance between the rectal wall and US probe increased and the rectal wall became less distinct (see Figure 2.3 and Figure 2.4).

Based on CT contouring alone, we found an inter-observer variability of 5.5% for prostate V_{100} and 10.3% for D_{90}. De Brabandere et al. [6] found considerably larger inter-observer variabilities (V_{100}: 11.7% and D_{90}: 23%) during their contouring study, performed by eight physicians from seven institutes. Comparing observers from a single institute was expected to result in smaller variabilities. The influence of institutional and personal habits on contouring is confirmed once again.

2.4.2 Registration

FMs cause bright artifacts on US and CBCT. This is in contrast to the signal voids that FMs cause in MRI scans. The localization on US is troublesome due to the artifacts caused by the implanted ^{125}I seeds. Seeds can be mistaken for FMs or FMs cannot be found at all. 68.2% of the selected FMs were considered correctly localized after outlier removal (false localization if Euclidean distance to the mean position $\geq$ 3 mm), whereas 91.3% were found during the registration process. During the registration procedure, finding the right FM is less difficult. Both US and CBCT (or MRI and CBCT) scans are visible at the same time, together with the root mean square (RMS). The RMS value describes the residual distance between the corresponding FMs on US and CBCT (or MRI and CBCT) after rigid transformation. A large RMS is often a sign of a false localization, which can be corrected immediately. This was not the case during the FM localization part of the multi-observer study.

Manual adjustment based on the urethra and the ^{125}I seeds is necessary for accurate US–CBCT registrations and compensates for the low FM visibility on US. The inter- and intra-observer variability are only slightly larger for US–CBCT registrations than for MRI–CBCT registrations (see Table 2.1). The lack of ^{125}I seeds and urethra visibility in the MRI scans made it more difficult to adjust the registration and resulted in less manual interactions (MRI–CBCT: 17.6% vs. US–CBCT: 78.4%).

Two important measures of prostate dosimetry are the V_{100} and D_{90}. Registration of T1 with CBCT resulted in an inter-observer variabilities of 1.3% for the V_{100} and 2.1% for the D_{90}. In the literature, a V_{100} variability of 2.9% based on CT-T1-T2 registration has been reported together with a D_{90} variability of 7% [6]. These variabilities based on multi-modality image registration are again larger than the variabilities found in our study. The smaller variabilities of our study originate from the fact that it is an intra-institute study.

Inter-observer DPs show significant differences between the US– and MRI–CBCT registrations. However, the mean difference between these two groups is -0.008 (V_{100}) and -0.006 (D_{90}). While statistically significant, these differences are not clinically relevant due to their small inter-observer variabilities (see SD_{clin} in Table 2.1).

2.4.3 Multi-observer study

During LDR treatment of the patient at the operating theater, it is possible to use the US probe for sagittal scans as well as continuous axial (or sagittal) scanning rather than slices with a fixed increment. This extra information can be used to more accurately determine the dimensions of the prostate (especially at the apex and base) and the organs at risk. This, together with the second independent radiation oncologist, will reduce the actual contouring variability in the clinical procedure.

US contouring introduces a larger inter- and intra-observer variability than either of the registrations. Therefore, contouring is the weaker link and should be improved before trying to

reduce the registration variabilities. The experienced radiation oncologists (observer 1 - 3) performed better than the inexperienced observers, who had larger geometric variabilities. Observer 4 received instructions from observer 1 once and performed better than the other two inexperienced observers. This demonstrates that training and guidelines can lead to better consensus in prostate contouring. A reduced inter- and intra-observer variability after three training sessions has been reported by Khoo et al. [36], even for experienced radiation oncologists. The effect of a training session just before performing a contouring study is expected to have a larger influence on inexperienced observers.

2.5 Conclusion

US– and MRI–CBCT registrations had to smaller variabilities than US and CT contouring, making contouring the weaker link. US contouring led to smaller geometrical variabilities as well as significantly smaller dosimetric variabilities than CT contouring. This makes US essential for prostate contouring and discourages CT contouring. Inter-observer contouring on US caused D_{90} variations of 9.3% from its clinical values. For all studies, intra-observer variabilities were smaller than inter-observer variabilities.

Good FM visibility on MRI scans resulted in small registration variabilities (inter-observer, prostate V_{100}: 1.3% and D_{90}: 2.1%). The inferior FM visibility on US, where only 68.2% of the FMs were considered correctly localized, was compensated by the manual adjustment based on the seed and urethra locations (inter-observer, prostate V_{100}: 2.0% and D_{90}: 3.1%). Manual adjustment of the US–CBCT registration is necessary to obtain an accurate registration. MRI–CBCT registration does not introduce more uncertainty than the currently performed US–CBCT registration and can therefore be used in our clinical setting. It is recommended to explore the incorporation of MRI scans in the LDR procedure.

Chapter 3

Source strength

3.1 Introduction

The manufacturer groups the seeds in batches based on their source strength. For each batch, a median source strength is reported together with a standard deviation. A bin width of ±2 - 8% around the median source strength is common [8]. This variation in source strength within a batch leads to changes in DPs.

Before implantation, the source strength of the delivered ^{125}I seeds is measured by the medical physicist assistant as part of the internal quality assurance procedure. These measurements are intended to verify that the batch with seeds was labeled and shipped correctly.

DeWerd et al. [28] investigated the dosimetric uncertainty for photon-emitting brachytherapy sources. Different variabilities within the manufacturing and quality assurance procedures were assessed for low- and high-energy sources. They find a calibration uncertainty of 1.3% for the air-kerma strength of low-energy photon-emitting sources.

Calibration should be performed with a measurement device that is traceable to the NIST (National Institute of Standards and Technology) standard [37]. Unfortunately, this is currently not possible at RISO. The AAPM and Netherlands Comission on Radiation Dosimetry (NCS) recommend calibration uncertainties below 3% [37, 38], where single seeds are allowed to exceed the specified activity by 5% or more. If a whole batch varies between 3 - 5%, this should be registered.

In this chapter, the variation of source strength within a batch is investigated by assessing the deviation between the measured and specified apparent activity. It is explored whether the measurement device at our institute performs within the guidelines of the NCS.

3.2 Materials and methods

At RISO, STM125I (Bard Brachytherapy, Inc., Carol Stream, IL, USA) seeds are used for permanent implants. The manufacturer reports an uncertainty of ±5% for these seeds.

The apparent activity of the ^{125}I seeds was measured with a well chamber (CRC-10; Capintec, Ramsey, NJ, USA). The well chamber is depicted in Figure 3.1a and a schematic drawing can be found in Khan [39, p. 324]. The source was placed in a plastic holder on the marked source position (see Figure 3.1c). The source position is marked in the holder to ensure the accurate and reproducible placement of the source in the center of the well chamber and therefore the correct geometry for the measurement.

(a) Well chamber

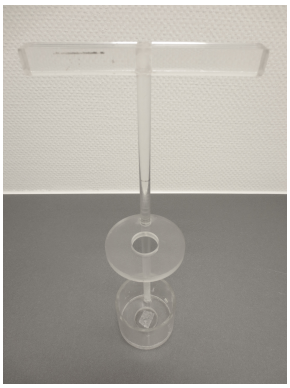

(b) Source holder

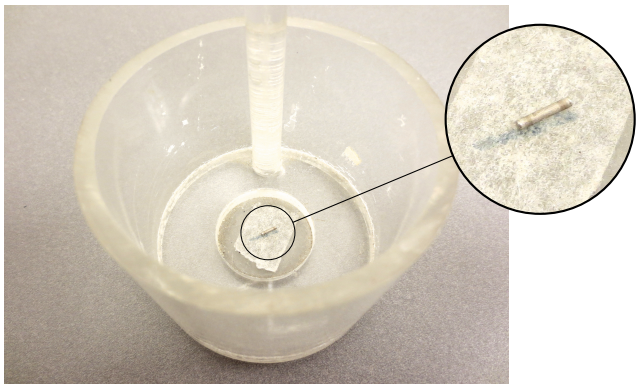

(c) ^{125}I seed in holder

Figure 3.1: (a) Well chamber and (b) source holder with (c) an ^{125}I seed used at RISO.

The manufacturer specified a certain initial apparent activity (A_0), which was then measured on average 3 days (range: 2 - 4) later at our institute. To account for the decay of the radioactive source, the apparent activity was recalculated for the day of the measurement. The law of radioactive decay was applied according to the following definition [40]:

$$A_t = A_0 \left(\frac{1}{2}\right)^{\frac{t-t_0}{T_{1/2}}} \tag{3.1}$$

With A_t as specified apparent activity at the measurement day, $t - t_0$ was the time between the initial calibration at the manufacturer and the measurement at our institute, and $T_{1/2}$ the half-life of ^{125}I. $T_{1/2}$ was specified by the manufacturer as 59.6 days in contrast to 59.43 days according to the NCS [38].

The deviation between the apparent activity specified by the manufacturer and the measured apparent activity was determined for five (separately packaged) seeds per patient. These five seeds were assumed to represent the whole batch of seeds that will be permanently implanted in the prostate of the patient. The measurement in the well chamber results in contamination of the sources and they could therefore not be used clinically.

The measurements performed for the LDR brachytherapy patients treated in 2014 were available to determine the uncertainty of the measurement device used at RISO. For each seed, the deviation (D_n) of the measured apparent activity (AM_n) with respect to the specified apparent activity (AS_n) was calculated according to Equation (3.2). This deviation was then averaged over the five seeds per patient. $D_n \geq 5\%$ were acceptable for single seeds within a batch. A batch was rejected when the average deviation was $\geq 5\%$ [38, 41].

$$D_n = \frac{AM_n}{AS_n} * 100 - 100 \tag{3.2}$$

The variability of the apparent activity (SD_A) was calculated with Equation (3.3) where N is the number of seeds measured.

$$SD_A = \sqrt{\frac{1}{N}\sum_{n=1}^{N}\left(\frac{AM_n}{AS_n} - 1\right)^2} \tag{3.3}$$

3.3 Results

During the measurements performed by the medical physicist assistant, the deviation from the specified apparent activity was calculated and averaged per batch to approve the seeds for implantation. A total of 364 seeds, intended for 73 patients, were measured with an average specified apparent activity of 0.483 mCi (range: 0.322 - 0.623) at the measurement day. None of the batches was rejected due to a too large deviation (average $D_n \geq 5\%$). 36 seeds (9.9% of the sources) had a deviation D_n of more than 5% from the specified apparent activity. For a single patient, only four seeds were measured for an unknown reason. All performed measurements can be seen in Figure 3.2. The measured apparent activity was on average 1.2% lower than the specified apparent activity. The seeds had a source strength variability (SD_A) of 3.0%, using Equation (3.3).

The seeds were divided into four groups according to their specified apparent activity. 60 seeds had a specified apparent activity below 0.400 mCi and presented with a SD_A of 2.8%. The 134 seeds with an apparent activity between 0.400 - 0.480 mCi had a SD_A of 3.1%. A larger SD_A

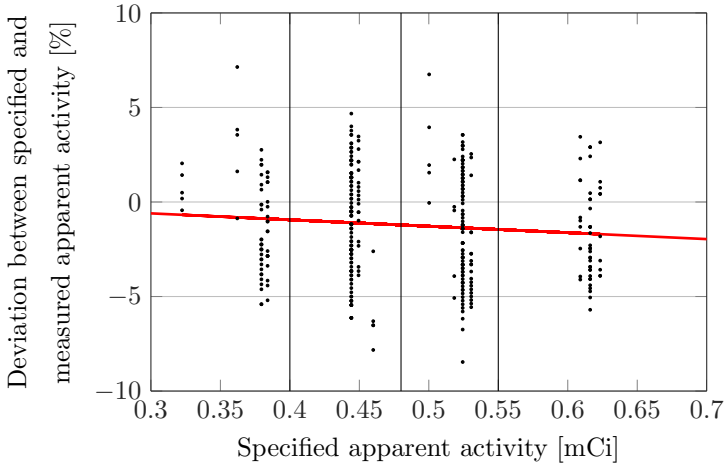

Figure 3.2: The deviation (D_n) between the specified and measured apparent activity of five seeds per patient treated in 2014. All measurements (●) are displayed together with the linear regression (–).
The seeds were divided into four groups based on their specified apparent activity.

of 3.2% was reached by the 120 seeds with a specified apparent activity of 0.480 - 0.550 mCi. The 50 seeds with a specified apparent activity above 0.550 mCi presented with a SD_A of 2.9%.

3.4 Discussion

A variability of 3.0% from the specified apparent activity was found and none of the batches was rejected due to too large deviations from the specified activity. According to DeWerd et al. [28], the uncertainty introduced by the clinical measurement of the source strength in a well chamber is 1.3% for low-energy photon-emitting sources. The AAPM [37] and NCS [38] recommend a calibration agreement between the clinical measurement and the manufacturer specifications of 3% within the batch mean and a maximum deviation of 5% from the mean. The variability (SD_A) of 3.0% is in agreement with this requirement. In addition, on average 1.2% lower apparent activities were measured. The measurement device is not traceable to a standard and it is therefore not possible to determine the definite cause of this deviation. The AAPM recommends source strength measurements with a measurement device that it traceable to a NIST standard [37]. In the Netherlands, there is no traceable standard available. A new measurement device that is traceable to a German standard is currently in the acquisition process. The used well chamber can then be calibrated with this traceable standard.

Only five (separately packaged) ^{125}I seeds were measured for each patient. It is assumed that these five seeds are a representation of the seeds that will be permanently implanted in the patient. It is not possible to measure the seeds that are about the be implanted because they have to remain sterile. Kutcher et al. [37] recommends the measurement of 10% of the seeds for quality assurance. At our institute, the number of measured seeds is set to five, independent of the number of implanted seeds. Implants generally consist of 60 - 80 seeds (see Westendorp et al. [16], Appendix A.1 Table A.1 and Appendix B.1 Table B.1). This would require 6 - 8 seeds. Due to regulations regarding the amount of stored radionuclides and financial considerations,

five seeds are ordered for the quality assurance measurements.

The calculated variability is only a small part of the uncertainty introduced by source strength. A detailed investigation of all aspects is beyond the scope of this thesis. DeWerd et al. [28] concluded a calibration uncertainty of 1.3% for the air-kerma strength. Kirisits et al. [8] combines the uncertainty of DeWerd et al. [28] with the source strength variation within a batch (2 - 8%, depending on the manufacturer) and concludes a source strength uncertainty of 1.4 - 2.6% for low-energy LDR sources like ^{125}I. They translate this to a D_{90} uncertainty of 3%. However, no literature was found that investigates the prostate D_{90} uncertainty based on the source strength uncertainty. A change in source strength does not necessarily lead to linear changes of the DPs due to the different placement of the seeds with respect to the target contours. The listed D_{90} uncertainty of 3% [8] would be a worst case scenario.

Keeping that in mind, the measurements performed with the well chamber at our institute do not lead to adjustments of the source strength uncertainty of Kirisits et al. [8] due to its agreement with the recommendations for clinical well chamber calibrations for low-energy photon-emitting brachytherapy sources. The change in source strength should be simulated in the clinical TPS to assess the dosimetric consequence of these source strength uncertainties.

3.5 Conclusion

Measured source strengths varied within 3.0% of the specified apparent activity. This agreement with the recommendation of 3% indicates that the measurement device can be used for the in-house quality assurance to verify correct labeling and shipment of the seeds.

The prostate D_{90} uncertainty level due to source strength (3%) Kirisits et al. [8] can be adopted for our institute as worst case scenario.

Part II

Sources of uncertainty:

Literature research

Chapter 4

Treatment planning

4.1 Treatment planning system

The TG-43 formalism introduced by the AAPM describes the dosimetry of brachytherapy sources [11, 12]. When implemented in the various TPSs, this formalism is often simplified and a set of parameters has to be chosen based on the look-up tables available in the literature [8, 42]. The simplifications and choice of parameters are a source of uncertainty.

DeWerd et al. [28] reports a total dose calculation uncertainty of 4.4% for low-energy photon-emitting brachytherapy sources like ^{125}I.

4.2 Medium dosimetric correction

Currently, the TG-43 formalism assumes the body as composed of only water [8, 11, 12]. However, it has been shown that tissue composition and density influence the absorbed dose. For low-energy sources like ^{125}I, the photoelectric effect is dominant and highly dependent on the atomic number of the irradiated tissue [17, 40, 43]. Current research uses Monte Carlo simulations to gain insight in the effect of different prostate-like tissue compositions [17, 43, 44].

Landry et al. [43] finds an average prostate D_{90} increase of 3.2% when investigating different prostate tissue compositions. Mass densities derived from CT reduced D_{90} by 2%. Carrier et al. [17] reports clinical target volume D_{90} that are on average 2.6% lower when accounting for tissue composition. In the review of Kirisits et al. [8], these uncertainties are combined to a D_{90} uncertainty of 5%.

4.3 Inter-seed attenuation

In the definitions of the TG-43 formalism, only a single source is considered [8, 11, 12], but an implant consist of about 60 - 80 seeds (see De Brabandere et al. [6], Westendorp et al. [16], and Appendix A.1 and B.1). Monte Carlo simulations with several seeds have been performed to investigate the change in DPs due to the interaction of the emitted photons with other seeds instead of the target tissue [17].

When accounting for inter-seed attenuation, clinical target volume D_{90} reduced by 4.1% [17]. Kirisits et al. [8] considers a prostate D_{90} uncertainty of 4% based on literature review.

Chapter 5

Treatment delivery imaging

The uncertainties regarding treatment delivery imaging include for example reconstruction uncertainties [8]. Two examples are the uncertainties introduced by seed localization and the resolution for dose calculation used in VariSeed.

5.1 Seed localization

In VariSeed, ^{125}I seeds can be automatically localized on CT scans. At RISO, this seed finder tool is used and the resulting seed distribution is visually checked and, if necessary, adjusted by the two radiation oncologists performing the implantation.

De Brabandere et al. [45] investigated the inter-observer variability of ^{125}I seed localization. Seven observers from six institutes localized seeds on CT and T1-weighted MRI scans of three patients with a schematic implant plan and post-implant X-rays available during the localization. Seed localization was performed manually on MRI while the observers were allowed to use the previously mentioned seed finder tool within VariSeed (Version 8.0) for the CT scans. Seed localization was CT-based for the dosimetry with CT alone and CT–T2 registration, while seed localization was MRI-based for the T1–T2 registration. They reported small inter-observer variabilities (1 SD with respect to the reference) for studies with a CT-based seed localization (prostate D_{90}: 1.3 and 1.5% and V_{100}: 0.5 and 0.9%) with a geometrical difference of 1.1 ± 0.5 mm between the reference and observer locations. MRI-based seeds localization, which was performed entirely manual, resulted in larger variabilities of 6.6% (D_{90}) and 2.8% (V_{100}) with a geometrical difference of 3.0 ± 0.9 mm between the reference and observer locations.

Comparable results were reported by Mangili et al. [46] when investigating the dosimetric consequences of seed localization at seven different institutes. The observers localized ^{103}Pd seeds on the CT scan of a single patient. They found a prostate V_{100} variability of 0.4% and a D_{90} variability of 1.7%.

5.2 Dose matrix resolution and DVH calculations

In the TPS, a DVH is calculated to obtain the DPs for the different structures. The resolution of the dose matrix can influence the dose volume histogram due to changes in contoured volume and a different dose per voxel.

Corbett et al. [21] investigated the influence of voxel size on several DPs and implemented the TG-43 formalism in Matlab. The results of their implementation were compared to dose calculations performed in VariSeed (Version 6.7) and calculations by hand. A single source was modeled and the DVH was calculated with the lowest possible resolution in VariSeed (0.5 mm in x- and y-direction). Compared to hand calculations, VariSeed calculated up to 50% lower values

for the volume of the isodose contours below 120 Gy and 50% larger values for the volumes of the isodose contours larger than 250 Gy. The recommendation of the American Brachytherapy Society (ABS) is a dose matrix resolution of 2 mm or less [47]. Corbett et al. [21] found small differences in RMS errors when gradually reducing the voxel size in VariSeed from 2 to 0.5 mm in the clinical plans of five patients with a prescribed dose of 145 Gy.

In order to obtain a DVH, volumes have to be calculated within the TPS. Each TPS does this in a different manner. Gossman et al. [22] compared DVH parameters of different TPSs with those according to the TG-43 formalism. A cuboid structure was defined in each TPS and its DVH was calculated. VariSeed overestimated the volume receiving a certain dose (1.5, 3.1, 7.1, 20.5 and 100.0% of the prescribed dose) by 0.4% (range: 0.2 - 0.6).

Kirisits et al. [42] compared the volumes computed in seven different brachytherapy TPSs. CT and MRI scans were made with one cone and two cylinder shaped phantoms. The contours within each TPS were approved by five observer to minimize inter-observer variabilities. The smallest dose matrix grid was used (0.5 mm in x-/y-direction and the z-resolution matched the slice spacing of 2 - 5 mm depending on the scan). VariSeed volumes were 1 - 8% larger than the volume averaged over the TPSs. For each scan evaluated in VariSeed, the cone showed the largest difference out of the three phantoms and the larger cylinder the smallest. Kirisits et al. [42] suggests that VariSeed overestimated the volumes because it includes the full length of the first and last contoured slice. Other TPSs round the edges when calculating the volumes in the last and first slice [42, 48]. The effect of inclusion or exclusion of the first and last slice was not quantified. Detailed information about the volume and DVH calculation algorithms within VariSeed is not available.

At RISO, the dose is calculated with a resolution of 1 mm in x- and y-direction while the resolution in z-direction matches the slice spacing (2.5 - 5 mm, depending on the modality). Based on the reviewed literature, it is not expected that a finer dose calculation grid will result in a more accurate dosimetry.

Chapter 6

Implant changes between implantation procedure and post-implant imaging

6.1 Seed migration and loss

Post-implant dosimetry takes place about 30 days after the implantation procedure [16]. During this Day 30 dosimetry, the ^{125}I seeds are visualized on a CT scan (CT 30). This CT scan is registered with the US scan acquired at the operating theater right before the implantation to obtain the DPs. It has been shown that seeds migrate between their insertion and the Day 30 dosimetry or can not be found on CT 30 [8, 14, 24]. Both seed migration and loss influence the dosimetry.

Fuller et al. [15] reported migration of 0.76% of the seeds when investigating 60 patients at Day 1 and at the 3 - 12 month follow up. The patients were treated with loose (37 patients, 5688 seeds) and stranded seeds (23 patients, 4018 seeds). Three of the stranded seeds showed distal migration along the path of the needle for more than 1 cm away from the main seed cluster. All three seeds, originating from two patients, migrated on Day 1. A total of nine seeds, originating from seven patients, migrated to the seminal vesicles. Three of these seeds migrated on Day 1.

Seed loss and migration was simulated by Knaup et al. [24] by removing the 1 - 3 seeds closest to the urethra and 1 - 3 seeds in the exterior of the prostate at different times after the implantation. Loose seeds close to the urethra are likely to be lost through the urethra and seed loss is expected to occur within the first few days. Removing the 1 - 3 seeds closest to the urethra within the first four days led to prostate D_{90} reductions of 2.6 - 9.1%. V_{100} reduced by 1.6 - 5.9%. Removing 1 - 3 peripheral seeds during the first 28 days led to D_{90} reductions of 1.3 - 2.9%. V_{100} reduced by 0.6 - 2.1%. Migration had smaller effects on the dosimetry than the described seed loss. Distal migration of the whole implant by 2 mm resulted in a D_{90} reduction of 1.2%.

At RISO, stranded seeds are used for the LDR procedure. Distal migration of stranded seeds has been reported when comparing Day 0 and Day 14 isodose lines with the location of the pubic bone and the prostate position [49]. The most common migration was the inferior movement of the whole implant. Prostate D_{90} decreased from 101 $\pm$ 21% of the prescribed dose to 97 $\pm$ 23%. V_{100} was 89.3 $\pm$ 7.8% and decreased to 87.1 $\pm$ 7.3%.

6.2 Edema

Another factor contributing to implant changes is edema. The needle insertion at the OR causes trauma and swelling of the prostate and the surrounding tissue.

Yue et al. [19] simulated edema by applying an exponential function to the radius of surface point of the prostate and thus isotropically contracting the prostate over time. This contraction, while resolving the edema, is applied to the seed location as well. An edema half-life of 9.3 days was chosen [50]. DVHs were calculated in 24 h increments for the first 30 days after implantation. Conventional plans overestimated prostate D_{90} by 4.4% when compared to edema corrected DVHs.

Saibishkumar et al. [25] reports prostate D_{90} of stranded seeds implants that were on average 154 Gy on Day 0 and 164 Gy on Day 30. When comparing Day 0 and Day 30 dosimetry, D_{90} increases of 13.1% have been reported together with Day 0 and Day 30 volumes that were respectively 36% and 9% larger than preplan volumes [51]. However, both studies did not correct for seed migration which could also lead to changes in dosimetry as previously mentioned.

Part III

Incorporation of MRI scans in LDR procedure

Chapter 7

Feasibility and dosimetry

7.1 Introduction

MRI provides superior soft-tissue contrast compared to US and CT [6, 7]. It is possible to visualize suspect lesion(s) in the prostate and define a boost area. For patients receiving a LDR boost after EBRT, the MRI scans (T1- and T2-weighted) are made 7 - 9 weeks prior to LDR treatment. The MRI scans are used for defining the target volume in EBRT treatment planning and are currently not used during the LDR part of the treatment. Incorporating these already available scans in the LDR procedure allows for the use of intraprostatic structures such as suspect lesions. Contours based on the US scans can be checked and the boost can be visualized on US and CBCT. Furthermore, accurate, quantitative dosimetry of the boost area is possible. The variability introduced by MRI–CBCT registrations has been investigated in the previously performed multi-observer study (see Chapter 2) and was smaller than the variability of the currently performed US–CBCT registration uncertainty.

In this chapter, it is investigated if and how the available MRI scans can be used in the clinically used TPS, VariSeed, during the implantation procedure. The time required for the additional registrations is determined. The dosimetry of the boost area is assessed at different moments of the implantation procedure.

7.2 Materials and methods

Seven patients (two T1c, two T2a, two T2b and one T2c) receiving LDR brachytherapy as a boost after EBRT were enrolled in this feasibility study. The patients received 47 Gy (20×2.35 Gy) during EBRT and 100 Gy during LDR brachytherapy. For these patient group, four gold FMs were implanted before EBRT treatment and the acquisition of the therapeutic MRI scans. T1- and T2-weighted MRI scans (Signa HDxt 3T, GE Medical, Milwaukee, WI, USA) were made on average 54 days (range: 48 - 63) prior to LDR treatment with a slice spacing of

Table 7.1: Scan parameters of the MRI scans.

	Sequence	Echo time [ms]	Repetition time [ms]	Echo train	Pixel Spacing [mm]
Axial T1	GR	3.12 - 3.32	250 - 300	1	0.45×0.45
Axial T2	SE	98.3 - 105.6	3675 - 4820	26 - 27	0.45×0.45

GR = Gradient Recalled; SE = Spin Echo.

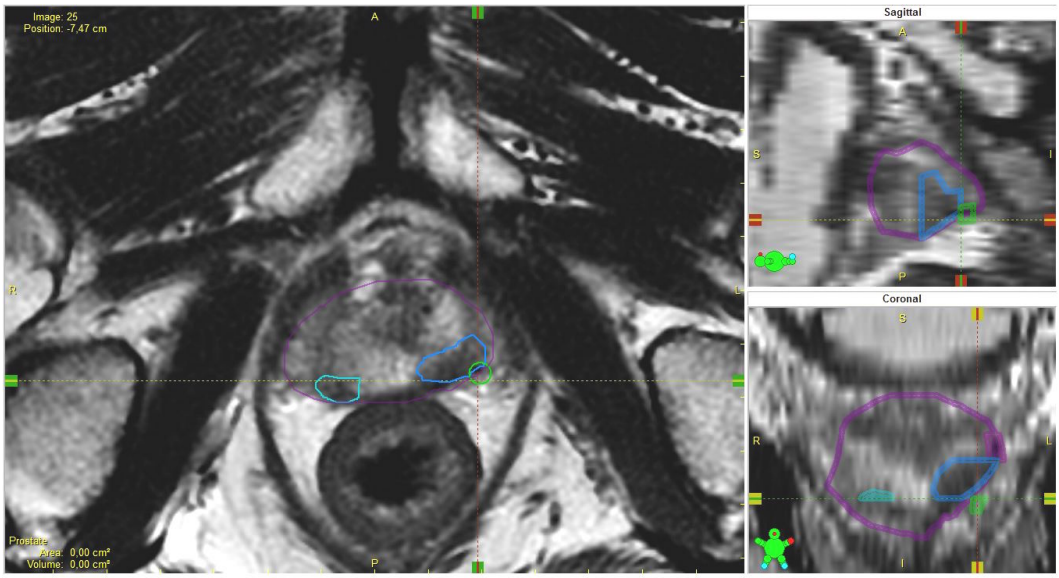

Figure 7.1: Contoured MRI study of patient 7 in VariSeed. $\text{Prostate}_{\text{MRI}}$ (magenta), Boost_1 (light blue) and Boost_2 (turquoise) contoured on T2 and a FM (green) localized on T1. Image blending is set to T2.

3.3 mm and a slice thickness of 3 mm. Additional parameters of the MRI scans can be found in Table 7.1.

A week before the LDR treatment, T1 and T2 were registered as a zero match in VariSeed. The treating radiation oncologist contoured the boost volumes based on T2 with the additional information from the radiology report and the diagnostic MRI scans. It is possible to contour two separate boost structures. In addition, the radiation oncologist contoured the prostate on T2. The four FMs were located on T1 due to its superior FM visibility compared to T2. The FMs were localized in the MRI study to simplify and shorten the registrations with MRI performed at the operating theater. The detailed instructions to prepare the MRI study can be found in Appendix B.2.

Each MRI study included:

- T1 and T2, registered as zero-match
- Boost_1 (and Boost_2) contours (based on T2)
- $\text{Prostate}_{\text{MRI}}$ contours (based on T2)
- FMs (localized on T1)

With the image blending tool, it can be gradually switched between T1 and T2. An example of the contoured MRI study can be seen in Figure 7.1.

At the operating theater, this MRI study was used twice. First, it was registered with US-pre, the pre-implant US made at the beginning of the implantation procedure with a FlexFocus 400 US system (BK Medical, Herlev, Denmark) and a slice spacing of 5 mm. US-pre was contoured (prostate, urethra, rectum and bladder) and then registered with the MRI study to transfer Boost_1 (and Boost_2) to US-pre and check the prostate contours of the US. During and after the

registration of US-pre with the MRI study, only T2 could be seen via image blending. T1 was no longer available due to limitations in VariSeed. The dosimetry of $Boost_1$ was visible throughout the update of the treatment plan, placement of needles and the ^{125}I seeds. $Boost_1$ V_{150} was added to the list of dosimetric quality alerts (in addition to the currently visible prostate V_{100} and D_{90}, urethra D_{30} and rectum V_{100}). The list within VariSeed is restricted to five dosimetric quality alerts, only allowing to visually follow the DP of one boost during the procedure. The radiation oncologist was instructed to contour the dominant lesion as $Boost_1$. Dosimetry of $Boost_2$ could be checked in the DVH in a different tab of VariSeed.

When all seeds were placed, the patients feet were lowered and US-post was acquired with an increment of 2.5 mm. Next, the leg support was removed and CT-post (Siemens Arcadis Orbic 3D; Siemens Medical Systems, Erlangen, Germany) was made with a slice spacing of 2.5 mm. The prostate and urethra were contoured on US-post and the seeds were automatically localized on CT-post. US–CBCT registration was performed to transfer the US-post contours to CT-post. Then, the CBCT was registered with the MRI study leading to a US–CBCT–T2 registration. The contours of the US study could be verified with the $Prostate_{MRI}$ contours and $Boost_1$ (and $Boost_2$) were transfered to the CBCT. An example can be seen in Figure 7.2. All structures could be seen on each of the three modalities. $Boost_1$ and $Boost_2$ V_{150} were assessed as the last step of the MRI incorporation.

The detailed instructions of the use of the MRI study at the OR can be found in Appendix B.3.

The volumes of $Prostate_{MRI}$, $Boost_1$ and $Boost_2$ were assessed on the MRI on which they were contoured. In addition, $Boost_1$ and $Boost_2$ volumes were determined after the registration of MRI with US-pre and after US–CBCT–MRI registration. Dosimetry was assessed pre-implant on US, immediately after implantation (post-implant, based on US only) and after US–MRI–CBCT registration.

7.3 Results

MRI was incorporated in the LDR procedure of seven patients. A summary of the findings is given in Table 7.2 and 7.3. With each patient, the procedure improved. The additional time needed for the registration with MRI was investigated in addition to the feasibility. During the first procedure, 10 min were needed for the US–MRI registration and another 10 min for the MRI–CBCT registration. These times were matched or lowered during the following patients, to about 10 min for both registration together.

The FM structures on T2 helped the radiation oncologists during the registrations at the OR because T1 was not visible while performing and evaluating the registrations. The caudal left FM could not be found on T1 of patient 4 and the caudal right FM on T1 of patient 6.

Differences between prostate contours based on US and MRI have been observed. $Prostate_{MRI}$ contours were smaller than US based contours, especially in the cranial direction at the interface of the bladder and prostate. A flattening of the prostate on US could be observed as well. Quantification was outside the scope of this study. At the operating theater, the $Prostate_{MRI}$ contour was not transferred to the US and CBCT to avoid a too full image with the isodose lines, that are not depicted in Figure 7.2 and 7.3.

Three of the seven patients had two dominant lesions (see Table 7.2). When treating patient 2, it was not yet possible to contour two boost regions as separate structures in VariSeed. The radiation oncologist contoured them with the same structure, leading to an interpolation between the two boosts. The two boost volumes were separated (contoured as individual $Boost_1$ and $Boost_2$) by the author after the implantation procedure.

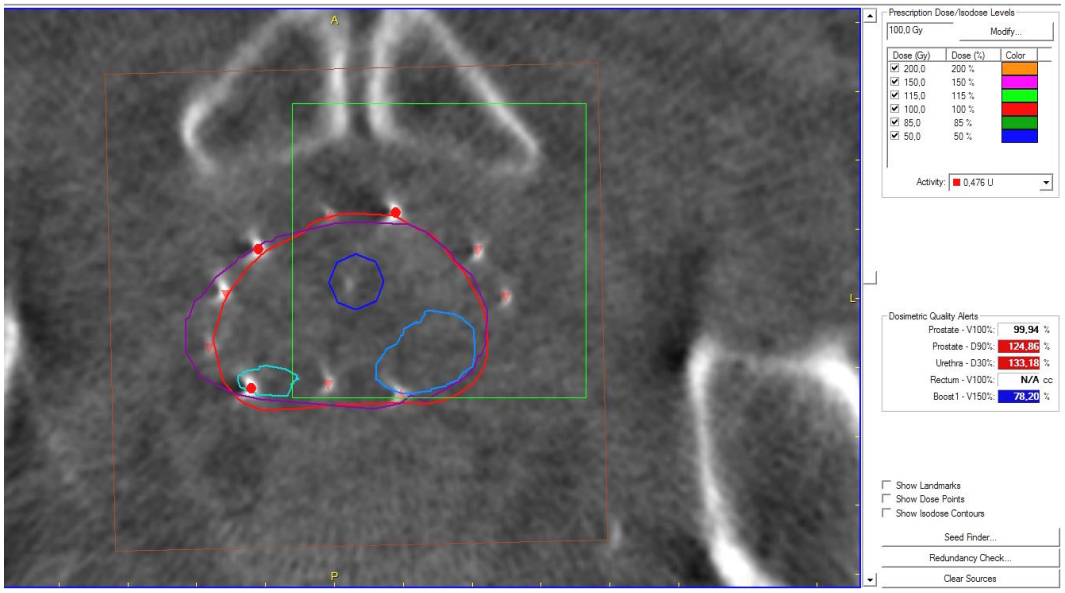

Figure 7.2: Contours from US and MRI transferred to CBCT for dosimetry of patient 7 in VariSeed. The prostate (red) and urethra (dark blue) were contoured on US-post, $\text{Prostate}_{\text{MRI}}$ (purple), Boost_1 (light blue) and Boost_2 (turquoise) were contoured on T2 and the seeds (● and ▼) were localized on CT-post. Image blending is set to CT-post and the isodose lines are not shown.

Table 7.2: Dosimetry of Boost_1 and Boost_2 after the registration of US-pre with MRI (pre-implant), immediately after implantation of all seeds (post-implant) and after the US–CBCT–MRI registration.

Patient	Boost_1 V_{150} [%]			Boost_2 V_{150} [%]	
	pre-impl.	post-impl.	reg.	post-impl.	reg.
1	–	75.6	91.4	–	–
2	–	–	87.6[a]	–	97.1[a]
3	–	97.5	100.0	–	–
4	–	83.7	72.5[b]	–	–
5	91.7	89.6	96.8	0[c]	100.0
6	64.5	73.0	84.0[b]	78.9	51.1[b]
7	95.1	98.1	78.2	100.0	100.0

– Not available.

[a] During procedure one combined boost. Separation into Boost_1 and Boost_2 performed by the author after the implantation procedure.

[b] Registration performed by the author after the implantation procedure.

[c] Boost contour in only one slice, volume of 0 cm^3.

Table 7.3: Volumes [cm^3] of $Prostate_{MRI}$, $Boost_1$ and $Boost_2$ on MRI, after registration with US-pre and after US–CBCT–MRI registration.

Patient	Prostate	$Boost_1$			$Boost_2$		
	MRI	MRI	US reg.	CBCT reg.	MRI	US reg.	CBCT reg.
1	–	3.3	2.6	3.0	–	–	–
2	36.8	0.91[a]	–	0.73[a]	0.54[a]	–	0.37[a]
3	50.5	3.5	2.3	2.8	–	–	–
4	18.0	5.8	3.5	5.2[b]	–	–	–
5	34.4	1.0	0.27	0.81	0.64	0.00[c]	0.38
6	27.1	1.7	0.67	1.4[b]	0.78	0.37	0.60[b]
7	28.1	1.6	0.66	1.3	0.30	0.16	0.15

– Not available.

[a] During procedure one combined boost. Separation into $Boost_1$ and $Boost_2$ performed by the author after the implantation procedure.

[b] Registration performed by the author after the implantation procedure.

[c] $Boost_2$ contour in only one slice, volume of 0 cm^3.

As visible in Table 7.2, not all steps were performed for each patient. For patient 2 for example, the US–MRI registration before seed placement was omitted due to a delay in the schedule. The MRI–CBCT registrations of patient 4 and 6 were performed by the author after the treatment because the radiation oncologists did not see an added value for the treatment of these two patients at the OR. Patient 4 had a transurethral resection of the prostate (TURP) prior to EBRT and LDR treatment. This led to a very small prostate and difficult US imaging. The radiation oncologists chose not to perform the MRI–CBCT registration. For patient 6, the MRI–CBCT registration was omitted due to inaccurate contouring of the boosts.

7.4 Discussion

7.4.1 Boost dosimetry

All patients received a satisfactory $Boost_1$ V_{150} (average 87.2%; range: 72.5 - 100.0) according to post-implant US–CBCT–MRI registration. The increase of V_{150} from pre- to post-implant dosimetry was expected since the dose distribution was shaped and refined throughout the procedure to ensure a suitable dose distribution with satisfactory DPs.

During LDR monotherapy, Gaudet et al. [18] shaped the 150% isodose line of 120 patients to include the dominant intraprostatic lesion and reached an average V_{150} of 94.9 $\pm$ 3.59%, with a prescribed dose of 144 Gy. The dominant intraprostatic lesion was defined based on sextant biopsies and contoured on US. They also found no significant differences between the 120 patients receiving a specified boost and the control group (70 patients) regarding acute (within 6 months) or late (follow-up of 3 years) toxicities. Cosset et al. [20] reported a boost V_{100} of 99.3% when treating only the focal volume (as defined by positive biopsies and MRI) with ^{125}I seeds and a prescribed dose of 144 Gy. The focal volume was on average 34% of the total prostate volume. In our study, the volume of the dominant lesion was on average 9.5% (range: 2.5 - 32.5) of the prostate volume. They compared the toxicities of the focal group with those of other patients treated with whole-gland LDR brachytherapy at the same institute. Similar to Gaudet et al. [18], there were no significant differences between focal and whole-gland LDR treatment.

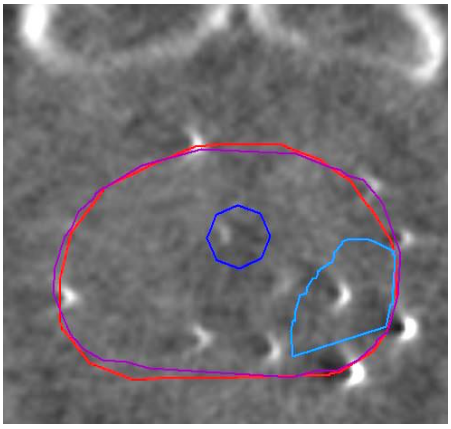

Figure 7.3: $Boost_1$ (light blue) is cut off after MRI–CBCT registration of patient 7. $Prostate_{MRI}$ (purple) and US based prostate (red) and urethra (dark blue) contours can be seen as well.

These two studies followed different approaches for focal brachytherapy; which can include additional boost constraints while still treating the whole prostate, hemigland therapy or treating only the focal region [52]. At our institute, MRI scans were used to assess and improve boost dosimetry while maintaining the whole prostate as primary treatment volume. Therefore, optimization of $Boost_1$ and $Boost_2$ V_{150} (as high as possible) had the lowest priority during the implantation procedure, after meeting prostate, urethra and rectum requirements. For dominant lesions in the posterior part of the prostate, the maximum rectum dose ($V_{100} < 1$ cm^3) was observed as a limiting factor. The DPs of each patient can be found in Table B.2 of Appendix B.1.

Currently, the radiation oncologist takes into account the dominant lesion by visually verifying the adequate dose coverage in that region during the update at the operation theater. This is done by subjectively examining the isodose contours and not related to certain parameters. During preplanning, the boost region is not considered at all. This implicit approach is therefore dependent on the judgment of the radiation oncologist and very subjective. The incorporation of MRI scans introduces an explicit, objective parameter for the dose coverage of the boost.

7.4.2 DVH calculations in VariSeed

For patient 7, boost dosimetry was optimized by placing one additional seed in each boost area. In the post-implant dose distribution on US, $Boost_1$ received an excellent V_{150} of 98.1% (see Table 7.2). After MRI–CBCT registration, $Boost_1$ V_{150} decreased to 78.2%. The volume of $Boost_1$ on the US during the implantation procedure was 0.66 cm^3 and $Boost_1$ contours appeared in two slices (slice spacing 5 mm). Only a small part (caudal, anterior) of the structure was not enclosed by the 150% isodose line. The volume of the initial $Boost_1$ structure on T2 was 1.6 cm^3, while appearing in four slices (slice spacing 3.3 mm). After CBCT–MRI registration, the $Boost_1$ volume (1.3 cm^3, contoured in four slices, slice spacing 2.5 mm) was in better agreement with the MRI volumes. The caudal anterior part of $Boost_1$ was not enclosed by the 150% isodose line. The boost dosimetry of the US directly after seed placement could be misleading due to reconstruction uncertainties of small structures (appearance in fewer slices, decreased volumes). These reconstruction uncertainties are assumed to originate from the different slice spacings between the scans since the volumes after US–CBCT–MRI registration were closer to the initial

MRI based volumes (see Table 7.3). Decreasing the slice spacing of the pre-implant US from 5 to 2.5 mm is expected to lead to better reconstructions of the small boost volumes after the registrations. The average difference between the volumes from US and CBCT registrations was 0.57 cm^3 (range: 0.01 - 1.7).

In addition, inconsistencies in the volume calculations in VariSeed were observed. When contouring a circular structure in a single slice in the US studies performed at the OR, study type "Intra-Operative Ultrasound Video Acquisition", the volume is 0 cm^3. Contouring in a second slice leads to a volume that is calculated as a cylinder with the height equal to once the slice spacing.

When contouring a circular structure in a single slice in the MRI or CBCT studies, study type "Post-Operative Image Import", the volumes are calculated as a cylinder with the height equal to once the slice spacing. When contouring a second slice, the volume is calculated as a cylinder with the height equal to twice the slice spacing. The same result is achieved when importing US scans as study type "Post-Operative Image Import".

This inconsistency has to be further investigated and reported to the manufacturer, Varian.

7.4.3 Contours

As mentioned in Section 7.3, a difference between US and MRI based prostate contours could be observed. The largest difference occurred at the cranial boundary of the prostate where the bladder begins. US prostate contours often include the bladder wall on MRI. Smith et al. [7] found US contours to be 1.5-3 mm larger than MRI contours. They also reported a flattening on the US compared to CT and MRI, which has been (subjectively) observed here as well.

The radiation oncologists noticed differences between US and MRI contours but did not adjust US contours based on their observations. The prostate is contoured larger at the base (towards the bladder) to ensure adequate dose coverage of the cranial prostate. Only boost contours were adjusted if they appeared outside the US prostate after registration. In addition, the boost structure had to be manipulated when the contour was cut off due the different angles between the scans during registration. An example can be seen in Figure 7.3 where $Boost_1$ was cut off.

For these seven patients, the therapeutic MRI scans (T1 and T2) were used during the implantation procedure. The diagnostic MRI could only be consulted outside the TPS while contouring T2; together with the radiology report based on the diagnostic MRI. This is an improvement from the current practice of referring to only descriptions in the radiology report to locate the boost area on US. When choosing for hormonal therapy to reduce the size of the prostate, T1 and T2 were taken after hormonal therapy has started. The dominant lesion could have decreased in size between taking the diagnostic MRI and the therapeutic MRI. However, it is still desired to treat the initial volume of the lesion with 150% of the prescribed dose.

7.4.4 Work flow in the clinical setting

During this feasibility study, the MRI study was prepared by the author and then contoured by the radiation oncologist a few days before the LDR procedure (see Appendix B.2 for the instructions). When implementing it in the clinical routine, the MRI study can be prepared and contoured together with the US study for treatment planning. The preparation (creating the new VariSeed studies, importing the Dicom data of the MRI scans and performing the zero match) will be a task for the brachytherapy technologists. The radiation oncologist can then contour structures in the MRI study when also contouring the US for preplanning. This way,

the second, independent radiation oncologist can check the contours on MRI while checking the contours on US.

The MRI contours of these patients have not been checked by the second, independent radiation oncologist. If $Boost_1$ and $Boost_2$ would have been checked by a second radiation oncologist, the contours of patient 6 would have been more accurate and the registration of US–CBCT–MRI would have been performed at the operating theater.

7.5 Conclusion

MRI scans have been successfully incorporated in the LDR procedure. An additional time of approximately 10 min at the operating theatre should be reserved for the registrations and about 15 min prior to the implantation procedure to contour the MRI study. This additional time is outweighed by the quantification of boost dosimetry and the definition of the boost boundaries The dominant lesion ($Boost_1$) received an average V_{150} of 87.2% (range: 72.5 - 100.0), based on post-implant US–CBCT–MRI registration at the operating theater.

The slice spacing and volume calculation of US-pre causes smaller boost volumes at the OR that can lead to incorrect DPs. Reducing the slice spacing of US-pre from 5 to 2.5 mm is expected to decrease these artifacts and should be explored before routinely incorporating the MRI scans in the LDR procedure.

Chapter 8

The effect of decreased US slice spacing on boost volumes

8.1 Introduction

MRI scans have been incorporated for seven patients treated with an LDR boost after EBRT treatment for prostate cancer (see Chapter 7). The large slice spacing of the pre-implant US (US-pre, 5 mm) caused decreased boost volumes while volumes after registration with the CBCT (slice spacing 2.5 mm) are in better agreement with the initial MRI based volumes. The volume changes also influence the calculated V_{150} and can lead to false conclusions. In addition, smaller voxels lead to more accurate DVHs since the dose matrix is calculated with a z-resolution that is equal to the slice spacing (see Chapter 5).

In this chapter, it is tested if a decreased slice spacing of US-pre will reduce the volume changes after the US–MRI registration and therefore result in a more accurate dosimetry of the dominant lesion(s) in the prostate.

8.2 Materials and methods

Three patients (one T2, one T2b and one T2c) treated with LDR brachytherapy after EBRT in December 2014 were examined. The patients received 47 Gy (20×2.35 Gy) during EBRT and 100 Gy during LDR brachytherapy. The MRI scans were delineated by the treating radiation oncologist prior to LDR treatment (see Section 7.2 and Appendix B for more details). For these patients, the $\text{Prostate}_{\text{MRI}}$, Boost_1 and Boost_2 contours were checked by a second radiation oncologist to ensure accurate contours.

At the operating theater, the patients were treated as described in Section 7.2. However, US-pre was obtained with 2.5 mm slice spacing (like US-post) instead of 5 mm.

The volumes of $\text{Prostate}_{\text{MRI}}$, Boost_1 and Boost_2 were assessed on the MRI on which they were contoured. In addition, Boost_1 and Boost_2 volumes were determined after the registration of MRI with US-pre and after US–CBCT–MRI registration. Dosimetry was assessed pre-implant on US, immediately after implantation (post-implant, based on US only) and after US–MRI–CBCT registration.

Table 8.1: Dosimetry of $Boost_1$ and $Boost_2$ after the registration of US-pre with MRI (pre-implant), immediately after implantation of all seeds (post-implant) and after the US–CBCT–MRI registration.

Patient	$Boost_1$ V_{150} [%]			$Boost_2$ V_{150} [%]	
	pre-impl.	post-impl.	reg.	post-impl.	reg.
1	98.5	98.9	99.5	–	–
2	90.5	86.3	96.6	–	–
3	100.0	92.0	100.0	40.6	86.6

– Not available.

Table 8.2: Volumes [cm^3] of $Prostate_{MRI}$, $Boost_1$ and $Boost_2$ on MRI, after registration with US-pre and after US–CBCT–MRI registration.

Patient	Prostate	$Boost_1$			$Boost_2$		
	MRI	MRI	US reg.	CBCT reg.	MRI	US reg.	CBCT reg.
1	44.7	1.9	1.4	1.6	–	–	–
2	65.4	4.2	2.8	2.6	–	–	–
3	14.9	0.69	0.45	0.52	0.71	0.44	0.47

– Not available.

8.3 Results

The US slice spacing was decreased for three patients while also incorporating the MRI scans during the implantation procedure. The dosimetry of the boost(s) can be seen in Table 8.1 and the $Prostate_{MRI}$ and boost volumes are given in Table 8.2. The average difference between boost volumes from US– and CBCT–MRI registrations was 0.15 cm^3 (range: 0.03 - 0.25). Additional DPs of the prostate, urethra and rectum can be found in Appendix B.1.

For patient 2 and 3, the boost volumes appeared outside the US-based prostate and had to be manually adjusted in location as well as size.

8.4 Discussion

MRI scans were successfully incorporated for three patients who received LDR brachytherapy after EBRT. A satisfactory $Boost_1$ V_{150} was reached for each patient. $Boost_1$ V_{150} after US–CBCT–MRI registration was 96.6% or higher.

Patient 2 and 3 presented with a large rectum on the MRI scans due to enclosed air (see Figure 8.1). The air led to deformation of the prostate and resulted in MRI based boost contours that appeared outside the prostate on the US at the operating theater. For both patients, the boost contours were adjusted in location and size by the radiation oncologist after the registrations. This step is of importance for the correct boost geometry and therefore dosimetry.

Due to the strict schedule at the MRI scanner, it is not possible to perform another MRI scan if there is air in the rectum. Therefore, prostate contours on the MRI should be compared to the US based contours during the LDR treatment at the OR. If a deformation of the prostate on MRI

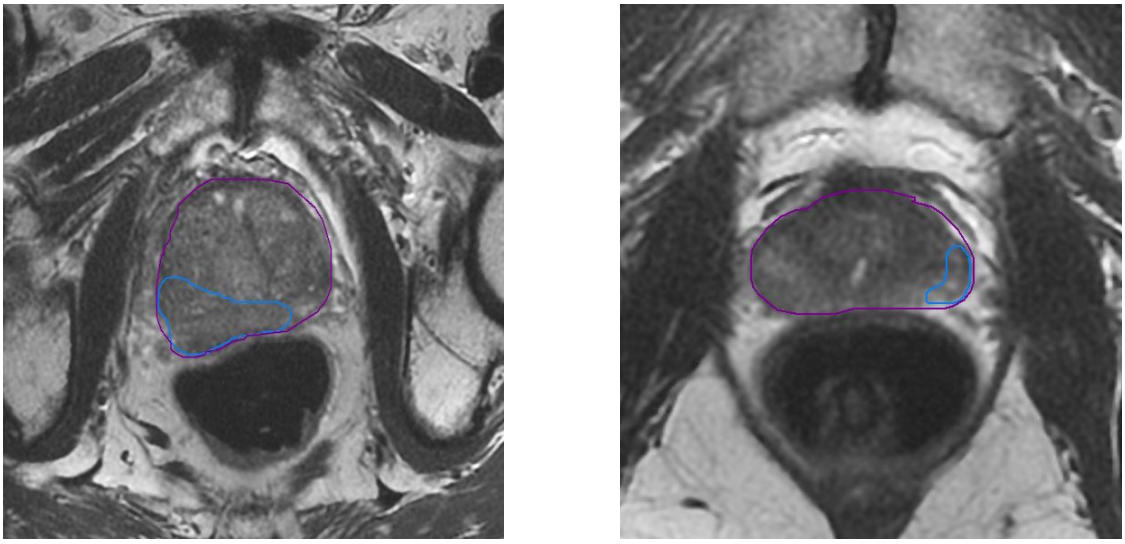

(a) Patient 2 (b) Patient 3

Figure 8.1: T2-weighted MRI scan of (a) patient 2 and (b) patient 3, including contours of $\text{Prostate}_{\text{MRI}}$ (magenta) and Boost_1 (light blue).

is visible, due to air or rectal filling, the boost structures should be adjusted accordingly. Despite the manual adjustment, the resulting quantified boost dosimetry is a valuable improvement to the current, entirely subjective, approach.

When comparing the boost volumes after US– and CBCT–MRI registration of the patients with larger US slice spacing (see Table 7.3) with the smaller US slice spacing (see Table 8.2), the differences between the two registration is lower with a smaller slice spacing. With the 5 mm slice spacing, the average difference between the volumes of the two registrations was 0.57 cm^3 (range: 0.01 - 1.7). This is lowered to 0.15 cm^3 (range: 0.03 - 0.25). However, only three patients were treated with a smaller US slice spacing. More patients should be investigated to confirm the decreased difference between boost volumes after US– and CBCT–MRI registration.

The additional time necessary to contour the extra slices was minimized by contouring only every second slice in the center of the prostate and each slice in the proximity of the base and apex. It is expected that the contouring variabilities, as assessed in Chapter 2, will decrease with the decreased slice spacing as well because the cranial and caudal parts had the largest variabilities.

Even though the volumes after registration with US and CBCT were in better agreement with each other, they are still not equal (see Table 7.3 and 8.2). The difference in volume calculation between the VariSeed study types is assumed to cause the remaining difference between boost volumes after US and CBCT registration (see Section 7.4.2 for explanations). The inconsistency in volume calculations applies to prostate volumes as well, but the effect is less distinct due to the larger volume of the prostate compared to the boosts. The remaining difference between volumes on MRI and after MRI–CBCT registration is assumed to originate from reconstruction artifacts after the registration.

8.5 Conclusion

The decreased slice spacing led to better agreement between the volumes after US– and CBCT–MRI registrations. A difference in volume calculation between the study types in VariSeed caused the remaining differences. The remaining difference with the MRI-based volumes is caused by reconstruction artifacts of the structures during the registration process. Boost volumes should be verified on the US and CBCT for their location and shape to prevent incorrect dosimetry. This is especially important for the small boost structures since they are prone to differences in volume calculation between the studies, movement between the imaging moments and reconstruction uncertainties during the registration.

The decreased slice spacing of 2.5 mm is advised for pre-implant US scans during the LDR treatment. It should be further investigated if the same results can be obtained with a larger group of patients. Decreasing the slice spacing of the pre-implant US scan during LDR monotherapy is recommended well.

Chapter 9

List of uncertainties

In the previous chapters, sources of uncertainty were investigated and quantified by experiments, simulations, and literature research. These uncertainties can be divided in two categories; intrinsic and extrinsic uncertainties. During this research, it is focused on intrinsic uncertainties, which are caused directly by the used techniques. These uncertainties are present throughout the LDR brachytherapy treatment due to the used techniques and do not change over the course of the treatment. Extrinsic uncertainties are related to the change of the implant geometry on patient level. During a single dosimetric evaluation, they are constant and do not have to be considered, but they change over the course of the treatment. For example, the seeds do not migrate while taking the post-implant US scan at the OR or the CT scan at Day 30, but in between these imaging moment there is seed migration. When assessing the dosimetry over time, extrinsic uncertainties have to be considered together with the intrinsic uncertainties.

A summary of the intrinsic and extrinsic uncertainties and their respective consequences for the prostate D_{90} and V_{100} can be found in Table 9.1 and 9.2, respectively. It is assumed that the sources of uncertainty are independent of each other. A combined D_{90} uncertainty of 13% is caused by the technique used for each dosimetric assessment of the implant. A 6% uncertainty is caused by changes on patient level. A combined D_{90} uncertainty of 14% was found for the LDR brachytherapy procedure of the prostate as implemented at RISO. US contouring had the largest uncertainty (9%) and is therefore the weakest link. The combined V_{100} uncertainties were not calculated since most reviewed literature did not include values for V_{100}.

Table 9.1: Intrinsic sources of uncertainty and their dosimetric consequences for prostate D_{90} and V_{100} during LDR brachytherapy treatment at RISO.

Source of uncertainty	Uncertainty [%]			Reference
	D_{90}	D_{90} [8]	V_{100}	
US contouring	9	2	2	Chapter 2
US–CBCT registration	3	–	2	Chapter 2
Source strength	3[a]	3	–	Kirisits et al. [8], DeWerd et al. [28]
Treatment planning system (VariSeed)	4	4	–	DeWerd et al. [28]
Medium dosimetric correction	3[a]	5	–	Kirisits et al. [8], Carrier et al. [17], Landry et al. [44]
Inter-seed attenuation	4	4	1	Carrier et al. [17]
Seed localization on CBCT	2	2[b]	1	De Brabandere et al. [45]
Dose matrix size and DVH calculations	1[a]	–[b]	–	Kirisits et al. [8], Corbett et al. [21], Kirisits et al. [42]
Combined standard uncertainty	13	9		

– Not available.

[a] Estimated value based on literature research and the estimate of Kirisits et al. [8].

[b] Seed localization and DVH calculations are combined to "Treatment delivery imaging" in the list of Kirisits et al. [8].

Table 9.2: Extrinsic sources of uncertainty and their dosimetric consequences for prostate D_{90} and V_{100} during LDR brachytherapy treatment at RISO.

Source of uncertainty	Uncertainty [%]			Reference
	D_{90}	D_{90} [8]	V_{100}	
Seed migration and loss of stranded seeds	4[a]	–[b]	3[a]	Kirisits et al. [8], Beaulieu et al. [14], Fuller et al. [15], Knaup et al. [24], McLaughlin et al. [49]
Edema	4	–[b]	–	Yue et al. [19]
Combined standard uncertainty	6	7[c]		

– Not available.

[a] Estimated value based on literature research and the estimate of Kirisits et al. [8].

[b] Listed together as "Implant changes between dose delivery and post-implant imaging" in Kirisits et al. [8].

[c] Estimated value based on expert discussion [8].

Chapter 10

Discussion

10.1 Uncertainties in the LDR procedure at RISO

The dominant uncertainty within LDR brachytherapy, target contouring, was quantified by own experiments; the multi-observer study in Chapter 2. Kirisits et al. [8] did not include the uncertainty of multi-modality image registration in his overview and listed a target contouring uncertainty of 2% based on CT or CT–T2 imaging. It is however unclear how they substantiate this value. The mentioned study of De Brabandere et al. [6] concludes inter-observer contouring variabilities of 23% based on CT alone and 17% based on CT–T2 imaging. Furthermore, assuming CT imaging is expected to result in larger uncertainties. During the multi-observer study, D_{90} varied within 10% of its clinical value due to CT contouring alone, whereas US contouring led to variations of 9%. A V_{100} uncertainty of 2% was determined at our institute. For comparison, this was 12% for CT imaging and 7% for CT–T2 imaging in the study performed by De Brabandere et al. [6].

As mentioned in Chapter 3, the uncertainty due to source strength is derived from literature and expressed in air-kerma strength. However, the same value is included as D_{90} level of uncertainty in the list of Kirisits et al. [8]. The influence of source strength variations on the DPs has not been substantiated in the literature and depends on the geometry of the implant, i.e. the location of the seeds with respect to the contours and the seed distribution itself. Similar to the dosimetric consequences of inter- and intra-observer contouring (see Chapter 2), the DPs do not have a linear response on changes in source strength. The source strength uncertainty of 3% is therefore an estimate and should be further explored and quantified.

It is of importance to assess the implant qualitatively as well as quantitatively. It is not possible to describe the dosimetry with a single parameter (here prostate D_{90}). Therefore, prostate V_{100} was included in the list of uncertainties. For each source of uncertainty, V_{100} had smaller levels of uncertainty than D_{90}. The largest D_{90} uncertainty of 9% due to contouring led to a V_{100} uncertainty of only 2%. This underlines the sensitivity of D_{90}. Both D_{90} and V_{100} should be consulted, together with a visual qualitative assessment of the isodose contours, to determine the quality of an implant and the implantation procedure in general.

A combined uncertainty of 14% was determined for the LDR procedure as implemented at RISO. The larger contouring uncertainty based on the multi-observer study resulted in a larger combined uncertainty, when comparing our uncertainties with the list of Kirisits et al. [8] (combined D_{90} uncertainty of 11%, see Table 9.1). The combined uncertainty of 14% is acceptable when considering the smaller V_{100} uncertainties as well. In addition, one should distinguish between systematic and random uncertainties. While some sources of uncertainty (e.g. inter-seed attenuation) lead to systematic over- or underestimation of the DPs, others (e.g. target contouring and multi-modality image registration) have a random nature.

10.2 Incorporation of MRI scans in LDR procedure

In Chapter 2, it was explored whether registration variabilities of US– and MRI–CBCT registrations were comparable. MRI–CBCT registrations had lower inter- and intra-observer variabilities than US–CBCT registrations. The incorporation of MRI scans in the LDR procedure was advised and the subsequent implementation was described in Chapter 7 and 8. The incorporation of MRI does not decrease the uncertainty of the procedure directly, but introduces boost dosimetry to it. In combination with a decreased pre-implant US slice spacing, it is possible to determine the dose given to the dominant lesion(s) in the prostate. The additional time necessary to prepare the MRI study, contour the larger amount of US slices and register the MRI with US-pre and CT-post is outweighed by the additional information obtained from the MRI. It leads to the possibility of super-boosting the dominant lesion with high accuracy. MRI scans will be routinely incorporated in the LDR procedure of patients with preceding EBRT.

The small volumes of the boost structures are prone to changes due to the different imaging moments and the registrations. At the OR, it should be verified whether Boost_1 (and Boost_2) are still located entirely within the prostate and their structures should be manually adjusted if deemed necessary.

Chapter 11

Conclusion

In Chapter 2, a multi-observer study was designed and performed to assess the inter- and intra-observer variability due to contouring and registration. US contouring alone resulted in a prostate D_{90} inter-observer variability of 9.3% and a geometrical inter-observer variability of 1.1 mm for the whole prostate. CT contouring led to larger variabilities (D_{90}: 10.3% and whole prostate: 1.9 mm) and is not recommended for prostate contouring. Registrations led to smaller variabilities than contouring and manual adjustment of US–CBCT registrations based on seed and urethra locations compensated for the poor FM visibility on US. US–CBCT introduced a D_{90} uncertainty of 3.1% and MRI–CBCT had an uncertainty of 2.1%.

The measured apparent activity varied within 3.0% of the specified apparent activity. This is in agreement with the requirements by the AAPM and NCS.

When reviewing the implementation of the TG-43 formalism, a dose calculation uncertainty of 4% was found when comparing the TG-43 formalism with the TPS. A D_{90} uncertainty of 3% is estimated based on literature review when accounting for prostate tissue composition. Depending on the tissue composition, D_{90} increased or decreased compared to water-like tissue. Accounting for the interaction between the emitted photons and the implanted seeds reduced D_{90} by 4%.

Seed localization on CT introduces a D_{90} uncertainty of 2%. The dose matrix resolution and DVH calculations have an estimated D_{90} uncertainty of 1% based on literature review.

Seed migration and seed loss of stranded seeds reduces D_{90} by 4% based on literature review. When accounting for edema, D_{90} reduces by 4%.

The LDR prostate brachytherapy procedure at RISO has a combined D_{90} uncertainty of 14% with US contouring (9%) as dominant uncertainty.

MRI scans were successfully incorporated in the LDR procedure in Chapter 7. The boost dosimetry can be followed throughout the procedure and $Boost_1$ V_{150} was on average 87%. The additional time of approximately 10 min necessary to register the MRI with US-pre and CT-post is outweighed by the quantification of boost dosimetry. The slice spacing of US-pre caused decreased boost volumes after the registration and an inconsistency in the volume calculation within VariSeed was revealed.

In Chapter 8, the pre-implant US slice spacing was reduced from 5 to 2.5 mm and the difference between boost volumes after US– and CBCT–MRI registration decreased.

Chapter 12

Recommendations and further directions

Based on the performed research, the sources of uncertainty in the LDR procedure as implemented at RISO were explored and quantified. In this chapter, recommendations are made to reduce or more accurately assess these uncertainties and improve the LDR procedure.

In Chapter 8, the slice spacing of the pre-implant US scan was decreased from 5 to 2.5 mm. The main goal was to improve boost volume reconstruction after the registration of MRI with US-pre, but it will also influence the contouring uncertainty investigated in Chapter 2. When implementing decreased US slice spacing in the standard clinical practice, contouring uncertainties in the cranial and caudal parts of the prostate are expected to reduce as well. The radiation oncologists contours the prostate on one extra slice even though it is not visible any more because the prostate ends in between the last slice with visible prostate tissue and the next. Contouring the extra slice, which does not include visible prostate tissue, ensures the proper dose coverage at these regions. Reducing the slice spacing from 5 to 2.5 mm will reduce the uncertainty regarding the craniocaudal dimensions of the prostate. Contouring an extra slice of 2.5 mm instead of 5 mm will decrease the overestimation of the prostate and therefore decrease the contouring variability. This could be investigated by letting observers contour the prostate on 2.5 mm US scans. After removing every second slice, thus creating a 5 mm US scan, the observers contour again. Comparing the two contours shows how the decreased US slice spacing affects the contouring uncertainty. The decreased pre-implant US slice spacing is recommended for all LDR patients.

The variability of source strength was quantified in our institute in terms of apparent activity in Chapter 3. Due to time limitations, it was not possible to quantify the effect of changes in apparent activity on the DPs (e.g. D_{90} and V_{100}). Source strength should be varied in clinical plans to assess the dosimetric consequences of the source strength variation within a batch.

Monte Carlo simulations are widely investigated to quantify the effect of tissue composition and inter-seed attenuation on the delivered dose (see Chapter 4). Medium dosimetric correction and inter-seed attenuation introduce large uncertainties (3 and 4%, respectively). Implementing the more accurate dose calculation algorithms into a clinically usable TPS would improve the assessment of the dose delivered to the target volume. This is particularly important for the LDR brachytherapy since the dominant interaction of the radiation with tissue, the photoelectric effect, is highly dependent on the atomic number. The current TG-43 formalism does not account for tissue heterogeneities like calcifications. These should be included in future Monte Carlo dose calculation algorithms as well.

Introducing Monte Carlo simulations in the clinical setting would also influence the uncertainties due to the implementation and simplification of the TG-43 formalism in the TPSs and

could possibly reduce the uncertainty of currently 4%.

MRI scans were incorporated for a total of ten patients and can be advised for patients with combined EBRT and LDR treatment. Incorporating MRI scans in the procedure is a first step towards a more focal treatment in the future and delivery of a super-boost to the dominant lesion. US slice spacing was decreased for only three patients of which two showed large deformations due to air in the rectum. More patients should be investigated to assess whether a decreased US slice spacing leads to smaller differences between US– and CBCT–MRI registrations for those patients as well.

Currently, MRI scans are acquired for LDR patients with preceding EBRT, but not for LDR monotherapy patients. It is recommended to investigate the benefit of MRI scans at the OR for these patients.

MRI scans are made for patients receiving HDR brachytherapy as well since HDR is always combined with a preceding course of EBRT. Incorporation of MRI scans in the HDR procedure should be explored since these patients are already treated with certain dosimetric constraints for the suspect lesion. This can be done more accurately by registrations with contoured MRI in the TPS.

Another problem is the volume calculation in VariSeed. In Chapter 5, the differences in volume calculations between TPSs was expressed. In addition, inconsistencies in volume calculation between the study types within VariSeed were observed during analysis of the boost volumes (see Chapter 7 and 8). This should be reported back to Varian and further investigated. Especially since it also influences the DPs of all structures during the intra-operative and Day 30 dosimetry.

References

[1] J. Ferlay, E. Steliarova-Foucher, J. Lortet-Tieulent, S. Rosso, J.W.W. Coebergh, H. Comber, D. Forman, and F. Bray. Cancer incidence and mortality patterns in europe: Estimates for 40 countries in 2012. *European Journal of Cancer*, 49(6):1374 – 1403, 2013.

[2] R. Siegel, J. Ma, Z. Zou, and A. Jemal. Cancer statistics, 2014. *CA Cancer Journal for Clinicians*, 64(1):9–29, 2014.

[3] B.R. Thomadsen, J.F. Williamson, M.J. Rivard, and A.S. Meigooni. Anniversary paper: Past and current issues, and trends in brachytherapy physics. *Medical Physics*, 35(10): 4708–4723, 2008.

[4] A. Polo. Image fusion techniques in permanent seed implantation. *Journal of Contemporary Brachytherapy*, 2(3):98–106, 2010.

[5] H. Westendorp, C.J. Hoekstra, A. van't Riet, A.W. Minken, and J.J. Immerzeel. Intraoperative adaptive brachytherapy of ^{125}I prostate implants guided by c-arm cone-beam computed tomography-based dosimetry. *Brachytherapy*, 6(4):231–237, 2007.

[6] M. De Brabandere, P. Hoskin, K. Haustermans, F. Van Den Heuvel, and F.-A. Siebert. Prostate post-implant dosimetry: Interobserver variability in seed localisation, contouring and fusion. *Radiotherapy and Oncology*, 104(2):192–198, 2012.

[7] W.L. Smith, C. Lewis, G. Bauman, G. Rodrigues, D. D'Souza, R. Ash, D. Ho, V. Venkatesan, D. Downey, and A. Fenster. Prostate volume contouring: A 3d analysis of segmentation using 3dtrus, ct, and mr. *International Journal of Radiation Oncology Biology Physics*, 67 (4):1238–1247, 2007.

[8] C. Kirisits, M.J. Rivard, D. Baltas, F. Ballester, M. De Brabandere, R. Van Der Laarse, Y. Niatsetski, P. Papagiannis, T.P. Hellebust, J. Perez-Calatayud, K. Tanderup, J.L.M. Venselaar, and F.-A. Siebert. Review of clinical brachytherapy uncertainties: Analysis guidelines of gec-estro and the aapm. *Radiotherapy and Oncology*, 110(1):199–212, 2014.

[9] A.J.G. Even. *Optimizing High-Dose-Rate Brachytherapy for the Prostate*. RISO and University of Twente, 2013.

[10] ICRU (International Comission on Radiation Units and Measurements). Dose and volume specification for reporting intracavitary therapy in gynaecology. ICRU Report 38, 1985.

[11] R. Nath, L.L. Anderson, G. Luxton, K.A. Weaver, J.F. Williamson, and A.S. Meigooni. Dosimetry of interstitial brachytherapy sources: Recommendations of the aapm radiation therapy committee task group no. 43. *Medical Physics*, 22(2):209–234, 1995.

[12] M.J. Rivard, B.M. Coursey, L.A. DeWerd, W.F. Hanson, M.S. Huq, G.S. Ibbott, M.G. Mitch, R. Nath, and J.F. Williamson. Update of aapm task group no. 43 report: A revised aapm protocol for brachytherapy dose calculations. *Medical Physics*, 31(3):633–674, 2004.

[13] M.J. Rivard, W.M. Butler, L.A. DeWerd, M.S. Huq, G.S. Ibbott, A.S. Meigooni, C.S. Melhus, M.G. Mitch, R. Nath, and J.F. Williamson. Supplement to the 2004 update of the aapm task group no. 43 report. *Medical Physics*, 34(6):2187–2205, 2007.

[14] L. Beaulieu, L. Archambault, S. Aubin, E. Oral, R. Taschereau, and J. Pouliot. The robustness of dose distributions to displacement and migration of ^{125}I permanent seed implants over a wide range of seed number, activity, and designs. *International Journal of Radiation Oncology Biology Physics*, 58(4):1298–1308, 2004.

[15] D.B. Fuller, J.A. Koziol, and A.C. Feng. Prostate brachytherapy seed migration and dosimetry: analysis of stranded sources and other potential predictive factors. *Brachytherapy*, 3 (1):10 – 19, 2004.

[16] H. Westendorp, R. Kattevilder, A. van't Riet, A.W. Minken, T.T. Nuver, J.J. Immerzeel, and C.J. Hoekstra. Objective automated assessment of time trends in prostate edema after ^{125}I implantation. *Brachytherapy*, 11(5):327–333, 2012.

[17] J.-F. Carrier, M. D'Amours, F. Verhaegen, B. Reniers, A.-G. Martin, E. Vigneault, and L. Beaulieu. Postimplant dosimetry using a monte carlo dose calculation engine: A new clinical standard. *International Journal of Radiation Oncology Biology Physics*, 68(4):1190–1198, 2007.

[18] M. Gaudet, E. Vigneault, S. Aubin, N. Varfalvy, F. Harel, L. Beaulieu, and A.-G. Martin. Dose escalation to the dominant intraprostatic lesion defined by sextant biopsy in a permanent prostate ^{125}I implant: A prospective comparative toxicity analysis. *International Journal of Radiation Oncology Biology Physics*, 77(1):153–159, 2010.

[19] N. Yue, A.P. Dicker, R. Nath, and F.M. Waterman. The impact of edema on planning ^{125}I and ^{103}Pd prostate implants. *Medical Physics*, 26(5):763–767, 1999.

[20] J.-M. Cosset, X. Cathelineau, G. Wakil, N. Pierrat, O. Quenzer, D. Prapotnich, E. Barret, F. Rozet, M. Galiano, and G. Vallancien. Focal brachytherapy for selected low-risk prostate cancers: A pilot study. *Brachytherapy*, 12(4):331 – 337, 2013.

[21] J.-F. Corbett, J. Jezioranski, J. Crook, and I. Yeung. The effect of voxel size on the accuracy of dose-volume histograms of prostate ^{125}I seed implants. *Medical Physics*, 29(6):1003–1006, 2002.

[22] M.S. Gossman, S.S. Hancock, R.J. Kudchadker, P.R. Lundahl, M. Cao, and C.S. Melhus. Brachytherapy dose-volume histogram commissioning with multiple planning systems. *Journal of Applied Clinical Medical Physics*, 15(2):110–120, 2014.

[23] C. Salembier, P. Lavagnini, P. Nickers, P. Mangili, A. Rijnders, A. Polo, J. Venselaar, and P. Hoskin. Tumour and target volumes in permanent prostate brachytherapy: A supplement to the estro/eau/eortc recommendations on prostate brachytherapy. *Radiotherapy and Oncology*, 83(1):3 – 10, 2007.

[24] C. Knaup, P. Mavroidis, C. Esquivel, S. Stathakis, G. Swanson, D. Baltas, and N. Papanikolaou. Investigating the dosimetric and tumor control consequences of prostate seed loss and migration. *Medical Physics*, 39(6):3291–3298, 2012.

[25] E.P. Saibishkumar, J. Borg, I. Yeung, C. Cummins-Holder, A. Landon, and J. Crook. Sequential comparison of seed loss and prostate dosimetry of stranded seeds with loose seeds in ^{125}I permanent implant for low-risk prostate cancer. *International Journal of Radiation Oncology Biology Physics*, 73(1):61–68, 2009.

[26] Mayo Foundation for Medical Education and Research. Permanent prostate brachytherapy, 2015. URL `http://www.mayoclinic.org/tests-procedures/prostate-brachytherapy/multimedia/PRC-20014309`. (last accessed on January 20, 2015).

[27] Joint Committee for Guides in Metrology (JCGM 100:2008). *Evaluation of measurement data - Guide to the expression of uncertainty in measurement*. International Organization for Standardization (ISO), corrected version 2010. URL `http://www.bipm.org/utils/common/documents/jcgm/JCGM_100_2008_E.pdf`. (last accessed January 14, 2015).

[28] L.A. DeWerd, G.S. Ibbott, A.S. Meigooni, M.G. Mitch, M.J. Rivard, K.E. Stump, B.R. Thomadsen, and J.L.M. Venselaar. A dosimetric uncertainty analysis for photon-emitting brachytherapy sources: Report of aapm task group no. 138 and gec-estro. *Medical Physics*, 38(2):782–801, 2011.

[29] B. Basel. *Visibility of fiducial marker on Magnetic Resonance Imaging*. RISO and University of Twente, 2012.

[30] J.G.M. Beijer. *Detectability and visibility of fiducial markers in prostate brachytherapy on ultrasound*. RISO and University of Twente, 2012.

[31] D. Bowes, J.M. Crook, C. Araujo, and D. Batchelar. Ultrasound-ct fusion compared with mr-ct fusion for postimplant dosimetry in permanent prostate brachytherapy. *Brachytherapy*, 12(1):38–43, 2013.

[32] D. Ash, B. Al-Qaisieh, D. Bottomley, B. Carey, and J. Joseph. The correlation between D_{90} and outcome for ^{125}I seed implant monotherapy for localised prostate cancer. *Radiotherapy and Oncology*, 79(2):185–189, 2006.

[33] R.G. Stock. Counterpoint: There is a dose-response relationship in the low-dose rate brachytherapy management of prostate cancer. *Brachytherapy*, 9(4):293–296, 2010.

[34] C. Rasch, I. Barillot, P. Remeijer, A. Touw, M. van Herk, and J. V Lebesque. Definition of the prostate in ct and mri: a multi-observer study. *International Journal of Radiation Oncology*Biology*Physics*, 43(1):57 – 66, 1999.

[35] T. Nyholm, J. Jonsson, K. Söderström, P. Bergström, A. Carlberg, G. Frykholm, C.F. Behrens, P.F. Geertsen, R. Trepiakas, S. Hanvey, A. Sadozye, J. Ansari, H. McCallum, J. Frew, R. McMenemin, and B. Zackrisson. Variability in prostate and seminal vesicle delineations defined on magnetic resonance images, a multi-observer, -center and -sequence study. *Radiation Oncology*, 8(1), 2013.

[36] E.L.H. Khoo, K. Schick, A.W. Plank, M. Poulsen, W.W.G. Wong, M. Middleton, and J.M. Martin. Prostate contouring variation: Can it be fixed? *International Journal of Radiation Oncology*Biology*Physics*, 82(5):1923 – 1929, 2012.

[37] G.J. Kutcher, L. Coia, M. Gillin, W.F. Hanson, S. Leibel, R.J. Morton, J.R. Palta, J.A. Purdy, L.E. Reinstein, G.K. Svensson, M. Weller, and L. Wingfield. Comprehensive qa for radiation oncology: Report of aapm radiation therapy committee task group 40. *Medical Physics*, 21(4):581–618, 1994.

[38] NCS (Netherlands Commission on Radiation Dosimetry). Dosimetry and quality control of brachytherapy with low-energy photon sources (^{125}I). Report 20, 2012.

[39] F.M. Khan. *The physics of radiation therapy.* Lippincott Williams & Wilkins, 2010. ISBN 978 0 7817 8856 4.

[40] A.J.J. Bos, F.S. Draaisma, and W.J.C. Okx. *Inleiding tot de stralingshygiëne.* SDU Uitgevers, 2007. ISBN 978 90 12 11 905 4.

[41] R. Nath, L.L. Anderson, J.A. Meli, A.J. Olch, J.A. Stitt, and J.F. Williamson. Code of practice for brachytherapy physics: Report of the aapm radiation therapy committee task group no. 56. *Medical Physics*, 24(10):1557–1598, 1997.

[42] C. Kirisits, F.-A. Siebert, D. Baltas, M. De Brabandere, T.P. Hellebust, D. Berger, and J. Venselaar. Accuracy of volume and dvh parameters determined with different brachytherapy treatment planning systems. *Radiotherapy and Oncology*, 84(3):290–297, 2007.

[43] G. Landry, B. Reniers, L. Murrer, L. Lutgens, E. Bloemen-Van Gurp, J.-P. Pignol, B. Keller, L. Beaulieu, and F. Verhaegen. Sensitivity of low energy brachytherapy monte carlo dose calculations to uncertainties in human tissue composition. *Medical Physics*, 37(10):5188–5198, 2010.

[44] G. Landry, B. Reniers, J.-P. Pignol, L. Beaulieu, and F. Verhaegen. The difference of scoring dose to water or tissues in monte carlo dose calculations for low energy brachytherapy photon sources. *Medical Physics*, 38(3):1526–1533, 2011.

[45] M. De Brabandere, B. Al-Qaisieh, L. De Wever, K. Haustermans, C. Kirisits, M.A. Moerland, R. Oyen, A. Rijnders, F. Van den Heuvel, and F.-A. Siebert. Ct- and mri-based seed localization in postimplant evaluation after prostate brachytherapy. *Brachytherapy*, 12(6):580–588, 2013.

[46] P. Mangili, L. Stea, F. Cattani, S. Lappi, F. Giglioli, E. Calamia, F. Ziglio, R. Martinelli, and B. Longobardi. Comparative study of permanent interstitial prostate brachytherapy post-implant evaluation among seven italian institutes. *Radiotherapy and Oncology*, 71(1):13–21, 2004.

[47] S. Nag, W. Bice, K. DeWyngaert, B. Prestidge, R. Stock, and Y. Yu. The american brachytherapy society recommendations for permanent prostate brachytherapy postimplant dosimetric analysis. *International Journal of Radiation Oncology Biology Physics*, 46(1):221–230, 2000.

[48] G.T. Herman, J. Zheng, and C.A. Bucholtz. Shape-based interpolation. *IEEE Computer Graphics and Applications*, 12(3):69–79, 1992.

[49] P. McLaughlin, V. Narayana, C. Pan, S. Berri, S. Troyer, J. Herman, V. Evans, and P. Roberson. Comparison of day 0 and day 14 dosimetry for permanent prostate implants using stranded seeds. *International Journal of Radiation Oncology Biology Physics*, 64(1):144–150, 2006.

[50] F.M. Waterman, N. Yue, B.W. Corn, and A.P. Dicker. Edema associated with ^{125}I or ^{103}Pd prostate brachytherapy and its impact on post-implant dosimetry: An analysis based on serial ct acquisition. *International Journal of Radiation Oncology Biology Physics*, 41(5):1069–1077, 1998.

[51] O. Tanaka, S. Hayashi, M. Matsuo, M. Nakano, H. Uno, K. Ohtakara, T. Miyoshi, T. Deguchi, and H. Hoshi. Effect of edema on postimplant dosimetry in prostate brachytherapy using ct/mri fusion. *International Journal of Radiation Oncology Biology Physics*, 69 (2):614–618, 2007.

[52] W.Y. Tong, G. Cohen, and Y. Yamada. Focal low-dose rate brachytherapy for the treatment of prostate cancer. *Cancer Management and Research*, 5(1):315–325, 2013.

Appendix A

Material of the multi-observer study

A.1 Patient data

Table A.1: Overview of patient data.

Patient	RISO ID	Number of ^{125}I seeds	Apparent activity per ^{125}I seed [mCi]	EBRT dose [Gy]	Brachytherapy dose [Gy]	US-CBCT	MRI-CBCT
01	060439AT1D	70	0.434	47	110	+	+
02	071242VU1H	74	0.512	47	110	+	–
03	091038ES1B	69	0.371	47	110	+	–
04	110161HA1P	71	0.434	47	110	+	+
05	121243VR1T	61	0.375	47	110	+	+
06	160339HU1K	58	0.375	47	110	+	+
07	180341ME1H	65	0.371	47	110	+	+
08	201138OG1H	63	0.375	47	110	+	+
09	230555WI1G	68	0.371	47	110	+	+
10	230643EN1J	65	0.371	47	110	+	–
11	251251TH1J	66	0.371	47	110	+	+

+ Available; – Not Available.

Table A.2: Dosimetric parameters (DPs) obtained with US–CBCT registration at the end of the implantation procedure of each patient and at the Day 30 dosimetry check. These DPs were used as reference for the evaluation of the observer registrations and contours, respectively.

	Patient										
	1	2	3	4	5	6	7	8	9	10	11
Prostate V_{100} [%]											
Registration	99.37	98.82	97.85	98.90	98.10	97.93	97.57	95.37	99.27	100.00	99.38
Day 30	99.06	98.35	98.59	98.88	99.61	96.87	99.57	96.71	99.07	100.00	99.93
Prostate D_{90} [%]											
Registration	116.15	108.94	110.17	109.68	109.94	107.37	122.51	108.71	116.52	115.59	122.47
Day 30	117.95	114.20	119.45	119.44	121.23	108.46	137.64	116.48	130.09	127.71	130.98
Urethra D_{30} [%]											
Registration	122.67	114.58	122.63	107.24	112.31	113.05	134.83	119.26	121.50	115.32	131.95
Day	128.31	132.57	136.97	126.12	128.91	131.89	153.79	132.57	154.65	128.62	145.87
Rectum V_{100} [cm^3]											
Registration	0.58	–	–	–	–	–	–	–	–	–	–
Day 30	2.10	0.81	0.34	0.64	0.34	0.39	0.01	3.25	1.02	0.04	0.14

– Not available.

A.2 Instructions for the first session

The following guide was given to the observers for performing the first session the multi-observer study:

Procedure

In de 'Patient Manager' van VariSeed staan alle patiënten en de in te vullen studies klaar. De volgende studies zijn per patiënt beschikbaar:

- contour_us voor het intekenen van contouren op de OK-pre US
- fm_us voor het intekenen van FMs op de OK-post 0,25 cm US
- contour_ct voor het intekenen van contouren op de dag 30 CT
- fm_ct voor het intekenen van FMs op de OK-post CBCT
- fm_mr voor het intekenen van FMs op de T1 MRI
- registratie_us voor de registratie van de OK-post CBCT en 0,25 cm US
- registratie_mr voor de registratie van de OK-post CBCT en T1 MRI

Verder heb je een uitgeprinte tabel gekregen om uitkomsten bij te houden en als dit van toepassing is commentaar te geven per patiënt (op bijvoorbeeld een scan o.i.d.). Voor drie patiënten zijn geen MRI scans beschikbaar; ook dit staat vermeld in de tabel.

Contouren op US
Open de studie contour_us. Teken hier de contouren van de prostaat, de blaas, de urethra en het rectum in. Sla de studie na het intekenen op en sluit hem.

FMs op US
Open de studie fm_us. Er zijn structuren beschikbaar voor de vier FMs (cra_li, cra_re, cau_li en cau_re). Markeer de FMs als de respectievelijke structuren door gebruik te maken van het brush tool van het contouring scherm. Het centrum van het cirkeltje moet overeen komen met het centrum van de FM. Wanneer het centrum van een FM tussen twee coupes in ligt, kan er op beide coupes de FM worden ingetekend. Van alle contourpunten wordt het centrum bepaald voor FM lokalisatie. FMs kunnen alleen in het transversale vlak geselecteerd worden. In het sagittale en coronale vlak geselecteerde FMs zijn niet te achterhalen in de dicom informatie.

Wanneer een FM niet te vinden is, vermeldt je de naam van de niet gevonden FM in de kolom 'FMs → US' van de tabel. Sla de studie op en sluit hem.

Contouren op CT
Open de studie contour_ct. Teken hier de contouren van de prostaat, de blaas en het rectum in. Sla de studie op en sluit hem.

FMs op CT
Open de studie fm_ct. Teken hier de FMs in zoals boven voor de US beschreven is. Vermeldt niet gevonden FMs met hun naam in de tabel in de kolom 'FMs → CT'.

FMs op MRI
Open de studie fm_mr. Teken hier de FMs in zoals boven voor de US beschreven is. Vermeldt niet gevonden FMs met hun naam in de tabel in de kolom 'FMs → MRI'.

US-CT registratie
Open de studie registratie_us. Voer de registratie uit tussen de CBCT beelden (inclusief al gelokaliseerde seeds) en de us belden aan de hand van de FMs. De US is al geïmporteerd en je moet allen via "Image Fusion → Register Image Volume" de registratie uitvoeren. Wanneer een FM op één van de twee scans niet te vinden is, vermeldt je dit in de tabel in de kolom 'US-CT registratie → FMs'. Vermeldt ook de naam van FMs die niet gebruikt worden voor de registratie. Vul eveneens de uiteindelijke RMS van de registratie in. Vermeldt hier verder of de registratie nog handmatig wordt aangepast, door gebruik van translatie en/of rotatie, na registratie a.d.h.v. de FMs in de kolommen onder 'Manual'. Importeer vervolgens alle 'Secondary Volume Structures'. VariSeed toont na de registratie dosimetrische parameter (let op dat de brachy dosis voor deze patiënten 110 Gy is i.p.v. de soms automatisch ingevulde 145 Gy), deze worden in de tabel ingevuld. Sla de studie op en sluit hem.

MRI-CT registratie
Open de studie registratie_mr. Voer de registratie uit tussen de CBCT beelden (inclusief al gelokaliseerde seeds) en de mr beelden aan de hand van de FMs zoals boven voor US-CBCT staat beschreven. Sla de studie op en sluit hem.

Laat alle patiënten en studies in de 'Patient Manager' staan en breng de laptop, samen met de ingevulde tabel, weer naar mij terug zodat ik de data kan exporteren en opslaan voor verdere verwerking in Matlab.

Bedankt voor je medewerking en tijd!

A.3 Instructions for the second and third session

The following instructions were given to the observer for performing the second and third session of the multi-observer study:

Procedure

In de 'Patient Manager' van VariSeed staan alle patiënten en de in te vullen studies klaar. De volgende studies zijn per patiënt beschikbaar:

- contour_us voor het intekenen van contouren op de OK-pre US
- fm_us voor het intekenen van FMs op de OK-post 0,25 cm US
- registratie_us voor de registratie van de OK-post CBCT en 0,25 cm US
- registratie_mr voor de registratie van de OK-post CBCT en T1 MRI

Verder heb je een uitgeprinte tabel gekregen om uitkomsten bij te houden en als dit van toepassing is commentaar te geven per patiënt (op bijvoorbeeld een scan o.i.d.). Voor drie patiënten zijn geen MRI scans beschikbaar; ook dit staat vermeld in de tabel.

Contouren op US
Open de studie contour_us. Teken hier de contouren van de prostaat, de blaas, de urethra en het rectum in. Sla de studie na het intekenen op en sluit hem.

FMs op US
Open de studie fm_us. Er zijn structuren beschikbaar voor de vier FMs (cra_li, cra_re, cau_li en cau_re). Markeer de FMs als de respectievelijke structuren door gebruik te maken van het brush tool van het contouring scherm. Het centrum van het cirkeltje moet overeen komen met het centrum van de FM. Wanneer het centrum van een FM tussen twee coupes in ligt, kan er op beide coupes de FM worden ingetekend. Van alle contourpunten wordt het centrum bepaald voor FM lokalisatie. FMs kunnen alleen in het transversale vlak geselecteerd worden. In het sagittale en coronale vlak geselecteerde FMs zijn niet te achterhalen in de dicom informatie.
Wanneer een FM niet te vinden is, vermeldt je de naam van de niet gevonden FM in de kolom 'FMs → US' van de tabel. Sla de studie op en sluit hem.

US-CT registratie
Open de studie registratie_us. Voer de registratie uit tussen de CBCT beelden (inclusief al gelokaliseerde seeds) en de us belden aan de hand van de FMs. De US is al geïmporteerd en je moet allen via "Image Fusion → Register Image Volume" de registratie uitvoeren. Wanneer een FM op één van de twee scans niet te vinden is, vermeldt je dit in de tabel in de kolom 'US-CT registratie → FMs'. Vermeldt ook de naam van FMs die niet gebruikt worden voor de registratie. Vul eveneens de uiteindelijke RMS van de registratie in. Vermeldt hier verder of de registratie nog handmatig wordt aangepast, door gebruik van translatie en/of rotatie, na registratie a.d.h.v. de FMs in de kolommen onder 'Manual'. Importeer vervolgens alle 'Secondary Volume Structures'. VariSeed toont na de registratie dosimetrische parameter (let op dat de brachy dosis voor deze patiënten 110 Gy is i.p.v. de soms automatisch ingevulde 145 Gy), deze worden in de tabel ingevuld. Sla de studie op en sluit hem.

MRI-CT registratie
Open de studie registratie_mr. Voer de registratie uit tussen de CBCT beelden (inclusief al gelokaliseerde seeds) en de mr beelden aan de hand van de FMs zoals boven voor US-CT staat beschreven. Sla de studie op en sluit hem.

Laat alle patiënten en studies in de 'Patient Manager' staan en breng de laptop, samen met de ingevulde tabel, weer naar mij terug zodat ik de data kan exporteren en opslaan voor verdere verwerking in Matlab.

Bedankt voor je medewerking en tijd!

A.4 Data sheets for the results of the multi-observer study

Each observer was given a data sheet for writing down results, further information and possible comments. These data sheets are shown in Figure A.1 for the first session and in Figure A.2 for the second and third session.

Gegevens		FMs			Commentaar		
		US	CT	MRI	Naam observer:	Herhaling:	Datum:
Naam	RISO ID	Locatie niet gevonden FMs	Locatie niet gevonden FMs	Locatie niet gevonden FMs			
At., D.	060439AT1D						
Vu., H.A.	071242VU1H			N/A			
Es., B.M.	091038ES1B			N/A			
Ha., P.A.M.	110161HA1P						
Vr., T.W.P.A	121243VR1T						
Hu., K.P.	160339HU1K						
Me., H.J.	180341ME1H						
Og., H.	201138OG1H						
Wi., G.	230555WI1G						
En., J.H.H.	230643EN1J			N/A			
Th., J.J.	251251TH1J						

Gegevens		US-CT registratie								
		FMs			Manual		Dosimetrische parameter			
Naam	RISO ID	RMS Error [mm]	Locatie niet gevonden FMs	Locatie niet gebruikte FMs voor registratie	Translatie	Rotatie	V100 [%]	D90 [%]	Urethra D30 [%]	Rectum V100 [cc]
At., D.	060439AT1D									
Vu., H.A.	071242VU1H									
Es., B.M.	091038ES1B									
Ha., P.A.M.	110161HA1P									
Vr., T.W.P.A	121243VR1T									
Hu., K.P.	160339HU1K									
Me., H.J.	180341ME1H									
Og., H.	201138OG1H									
Wi., G.	230555WI1G									
En., J.H.H.	230643EN1J									
Th., J.J.	251251TH1J									

Gegevens		MRI-CT registratie								
		FMs			Manual		Dosimetrische parameter			
Naam	RISO ID	RMS Error [mm]	Locatie niet gevonden FMs	Locatie niet gebruikte FMs voor registratie	Translatie	Rotatie	V100 [%]	D90 [%]	Urethra D30 [%]	Rectum V100 [cc]
At., D.	060439AT1D								N/A	
Ha., P.A.M.	110161HA1P								N/A	
Vr., T.W.P.A	121243VR1T								N/A	
Hu., K.P.	160339HU1K								N/A	
Me., H.J.	180341ME1H								N/A	
Og., H.	201138OG1H								N/A	
Wi., G.	230555WI1G								N/A	
Th., J.J.	251251TH1J								N/A	

Figure A.1: Data sheet for the first session of the multi-observer study.
N/A = Not Available.

Gegevens		FMs	Commentaar		
		US	Naam observer:	Herhaling:	Datum:
Naam	RISO ID	Locatie niet gevonden FMs			
At., D.	060439AT1D				
Vu., H.A.	071242VU1H				
Es., B.M.	091038ES1B				
Ha., P.A.M.	110161HA1P				
Vr., T.W.P.A	121243VR1T				
Hu., K.P.	160339HU1K				
Me., H.J.	180341ME1H				
Og., H.	201138OG1H				
Wi., G.	230555WI1G				
En., J.H.H.	230643EN1J				
Th., J.J.	251251TH1J				

Gegevens		US-CT registratie								
		FMs			Manual		Dosimetrische parameter			
Naam	RISO ID	RMS Error [mm]	Locatie niet gevonden FMs	Locatie niet gebruikte FMs voor registratie	Translatie	Rotatie	V100 [%]	D90 [%]	Urethra D30 [%]	Rectum V100 [cc]
At., D.	060439AT1D									
Vu., H.A.	071242VU1H									N/A
Es., B.M.	091038ES1B									N/A
Ha., P.A.M.	110161HA1P									N/A
Vr., T.W.P.A	121243VR1T									N/A
Hu., K.P.	160339HU1K									N/A
Me., H.J.	180341ME1H									N/A
Og., H.	201138OG1H									N/A
Wi., G.	230555WI1G									N/A
En., J.H.H.	230643EN1J									N/A
Th., J.J.	251251TH1J									N/A

Gegevens		MRI-CT registratie								
		FMs			Manual		Dosimetrische parameter			
Naam	RISO ID	RMS Error [mm]	Locatie niet gevonden FMs	Locatie niet gebruikte FMs voor registratie	Translatie	Rotatie	V100 [%]	D90 [%]	Urethra D30 [%]	Rectum V100 [cc]
At., D.	060439AT1D								N/A	
Ha., P.A.M.	110161HA1P								N/A	
Vr., T.W.P.A	121243VR1T								N/A	
Hu., K.P.	160339HU1K								N/A	
Me., H.J.	180341ME1H								N/A	
Og., H.	201138OG1H								N/A	
Wi., G.	230555WI1G								N/A	
Th., J.J.	251251TH1J								N/A	

Figure A.2: Data sheet for the second and third session of the multi-observer study. N/A = Not Available.

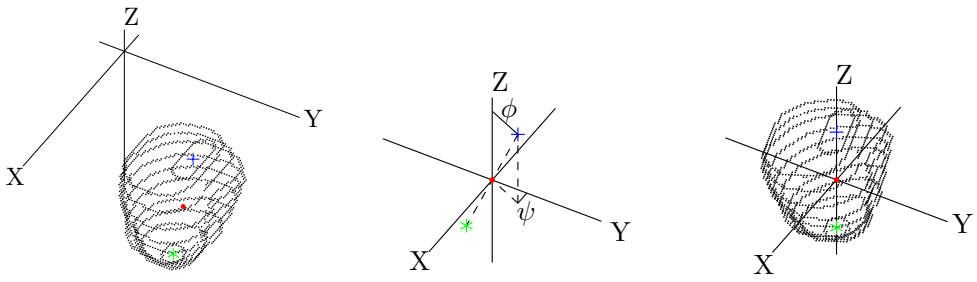

(a) Initial contours (b) After translation (c) Contours after translation and rotation

Figure A.3: Translation and rotation of the clinical prostate contour of patient 1 on US. The center (C_p,●) between the center of the base (B_p,+) and apex (A_p,✳) is translated to the origin of the coordinate system. Rotation with ψ around the z-axis and rotation with ϕ around the x-axis aligns the center of the base (B_p,+) on the positive z-axis.

A.5 Processing of the prostate contours

VariSeed exports 32 contour points for each contoured slice of prostate. Linear interpolation was applied to obtain closed contour lines with a resolution of 0.1×0.1×0.1 mm, which is below the smallest image resolution (US-pre: 0.12×0.12×5 mm, US-post: 0.12×0.12×2.5 mm, CBCT: 0.50×0.50×2.5 mm, CT 30: 0.35×0.35×2 mm and MRI: 0.47×0.47×2 mm).

Sample points had to be taken to geometrically compare the clinical contours with the observer contours. Before taking the samples, the prostate contours had to be translated and rotated such that the center of the rather small contoured apex (A_p) and base (B_p) were both on the z-axis (see Figure A.3a). The translation took place to set the center (C_p) of B_p and A_p in the origin of the coordinate system:

$$C_p = \frac{B_p - A_p}{2} \tag{A.1}$$

The center of the first and last slice of the patients scan, B_p and A_p, were rotated onto the positive respectively negative z-axis. This was achieved by rotation around the z-axis aligning B_p and A_p in the y-z-plane and then rotating the prostate around the x-axis so A_p and B_p lied on the z-axis. The rotation was described with the following rotation matrix that was applied to each contour point:

$$rot_p = \begin{bmatrix} \cos\psi & \cos\phi\sin\psi & \sin\phi\sin\psi \\ -\sin\psi & \cos\phi\cos\psi & \sin\phi\cos\psi \\ 0 & -\sin\phi & \cos\psi \end{bmatrix} \tag{A.2}$$

The angles ψ and ϕ were the azimuth and elevation necessary to align B_p on the positive z-axis (see Figure A.3b). C_p gave the position of the new origin in the coordinate system of the scan. Together with the rotation matrix rot_p, it was calculated for each patient's clinical contours and applied for the processing of all observer contours of that patient.

Appendix B

Material of MRI in LDR procedure

B.1 Patient data

Table B.1: Overview of patient data.

Patient	RISO ID	Number of ^{125}I seeds	Apparent activity per ^{125}I seed [mCi]	EBRT dose [Gy]	Brachytherapy dose [Gy]	US-pre slice spacing [mm]
01	280254SM1R	67	0.375	47	100	5.0
02	160343RO1A	64	0.439	47	100	5.0
03	100553KO1C	69	0.434	47	100	5.0
04	051138RE1A	55	0.311	47	100	5.0
05	030548ZW1J	66	0.375	47	100	5.0
06	080441SI1C	60	0.370	47	100	5.0
07	231150WE1A	60	0.375	47	100	5.0
08	110643KO1W	65	0.434	47	100	2.5
09	020341KO1J	63	0.518	47	100	2.5
10	061258WI1H	48	0.315	47	100	2.5

Table B.2: Dosimetric parameters at the end of the implantation, based on US only, after US–CBCT–MRI registration at the operating theater and at the Day 30 dosimetry. US-pre slice spacing was decreased from 5 to 2.5 mm for patient 8 - 10.

	Patient									
	1	2	3	4	5	6	7	8	9	10
Prostate V_{100} [%]										
Post-implant	99.90	99.68	99.61	98.33	99.84	99.50	100.00	100.00	99.75	98.95
Registration	99.77	98.48	99.65	94.44[a]	99.04	96.40[a]	99.94	99.46	99.28	98.80
Day 30	99.99	97.77	99.41	98.13	98.24	98.34	99.41	98.10	–	99.24
Prostate D_{90} [%]										
Post-implant	125.35	118.42	119.34	118.08	126.73	119.32	127.08	122.72	113.97	117.81
Registration	123.20	115.10	116.20	106.46[a]	124.21	110.87[a]	124.86	118.94	120.25	120.55
Day 30	139.81	125.00	129.95	118.12	129.69	117.21	132.63	110.91	–	121.75
Urethra D_{30} [%]										
Post-implant	123.71	117.96	121.45	119.46	122.44	118.10	126.36	121.46	120.11	119.82
Registration	128.87	129.35	129.41	112.30[a]	122.11	124.82[a]	133.18	120.49	124.22	139.88
Day 30	149.93	167.06	164.27	133.39	145.14	133.13	151.91	122.08	–	158.57
Rectum V_{100} [cm^3]										
Post-implant	0.28	0.87	0.62	0.00	0.51	0.99	0.59	0.18	1.38	1.20
Registration	–	–	–	–	–	–	–	0.52	3.31	–
Day 30	1.03	1.47	0.21	0.04	0.00	1.74	0.76	0.19	–	0.39

– Not available.

[a] Performed by the author after the implantation procedure.

B.2 Instructions for the preparation of the MRI study in VariSeed

- *Auteur (in klinische praktijk mogelijk taak van de radiotherapeutisch laborant):*
- Maak in VariSeed een nieuwe studie aan onder de naam “T1” (als post-OK image import)
- Importeer de T1 MRI scans
- Sla de “T1” studie op en ga terug naar de Patient Manager
- Maak in VariSeed een nieuwe studie aan onder de naam “MRI” (als post-OK image import)
- Importeer de T2 MRI scans
- Sla de “MRI” studie op
- Fuseer de T2 scan met “T1” via “Image Fusion” (als zero match)
- Noem het secondary image volume “t1” en selecteer “align centroids” in het “Manual” tabblad van de registratie
- Controleer of de twee MRI scans daadwerkelijk een zero match zijn m.b.v. “Image Blending”
- *Radiotherapeut-oncoloog:*
- Teken op basis van de T1 (secondary image volume) de FMs in
  - Voor het intekenen van de FMs worden per FM de uiteinden geselecteerd met de kwast

  - De FM moet in meer dan één coupe ingetekend zijn (zoals de groene intekening hieronder) omdat hij anders enkel als streepje in de sagittale en coronale vlakken verschijnt bij de registratie met CBCT of US

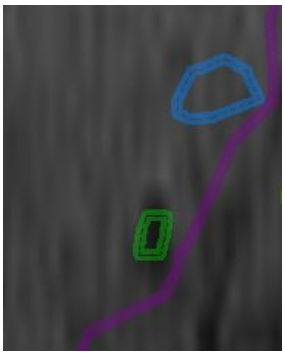

- Teken nu op de T2 (primary image volume) Boost_1 (en Boost_2) en $\text{Prostate}_{\text{MRI}}$ in

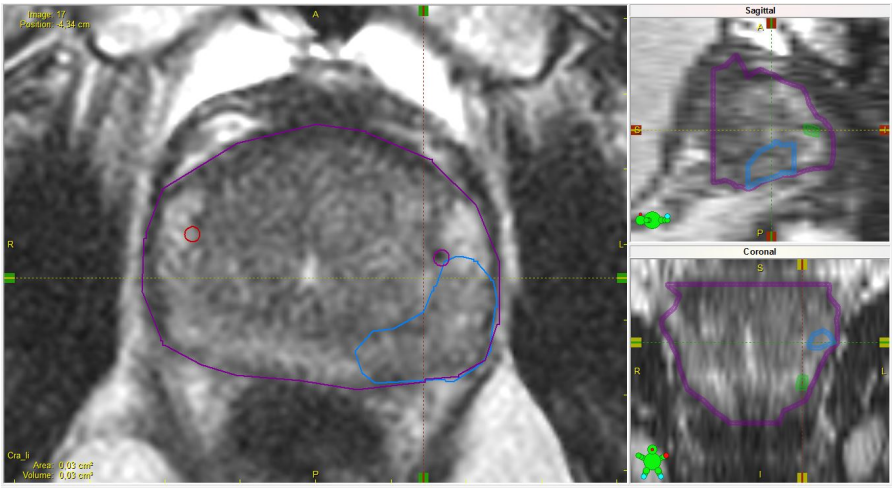

Figure B.1: Ingetekende MRI studie van patient 8 in VariSeed. $\text{Prostate}_{\text{MRI}}$ (paars), Boost_1 (lichtblauw) ingetekend op T2 en FMs (rood, magenta en groen) gelocaliseerd op T1. Image blending staat op T2.

- *Auteur (in klinische praktijk mogelijk taak van de radiotherapeutisch laborant):*
- Archiveer "MRI" naar de map J:\Brachy\DATA\VARISEED\OK

De volgende aanpassingen moeten één keer worden uitgevoerd voor elke VariSeed laptop:

- Maak "Structures" aan voor de boost, $\text{Prostate}_{\text{MRI}}$ en de vier fiducial markers (FMs)
- Boost kleuren:
  - Boost_1: Vierde rij van boven en tweede vakje van links
  - Boost_2: Vierde rij van beneden en eerste vakje van links
- $\text{Prostate}_{\text{MRI}}$ kleur: Derde rij van boven en eerste vakje van rechts
- FM kleuren:
  - Cra_{li}: Derde rij van beneden en vierde vakje van links
  - Cra_{re}: Tweede rij van boven en eerste vakje van links
  - Cau_{li}: Tweede rij van boven en vierde vakje van links
  - Cau_{re}: Tweede rij van boven en vijfde vakje van links

B.3 Instructions for the use of the MRI study at the operating theatre

- *Na het intekenen van US-pre:*
- Registeer US-pre met de MRI studie via "Image Fusion" → "Import Image Volume"
- Noem het nieuwe volume "mri" en klik "OK"

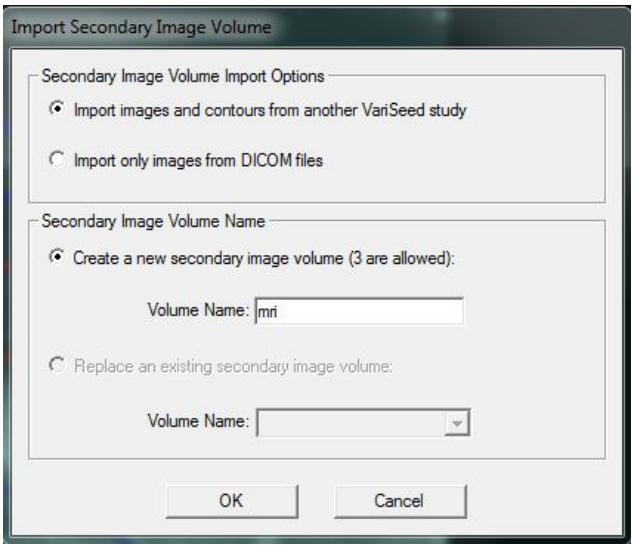

- Kies "MRI" als secondary structure en klik "OK"
- Klik "Register"

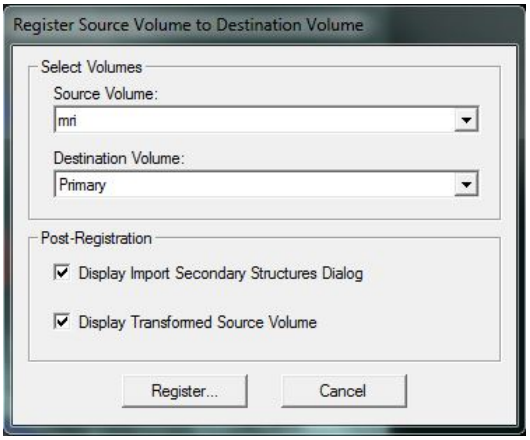

- Voer de registratie op basis van de FMs uit en, indien nodig, pas de registratie handmatig aan d.m.v. translatie en/of rotatie
- Vergelijk de prostaat contouren van de US met de contouren van de MRI

- Klik "OK" om de uiteindelijke registratie te accepteren
- Importeer Boost_1 (en Boost_2) door de structuur te slecteren en op het pijltje te klikken

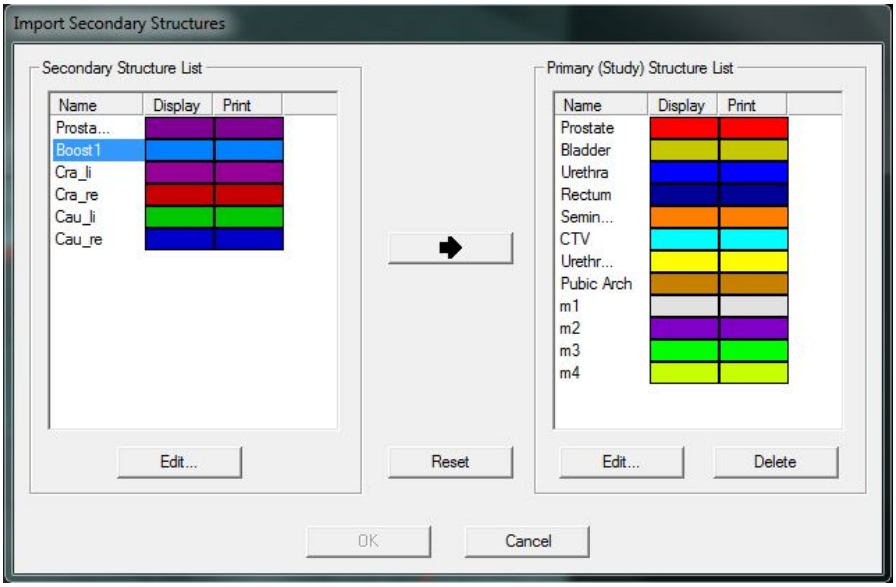

- Contoleer of de boost volumes binnen te prostaat liggen en niet afgeknipt werden door de registratie. Pas de contour desnoods aan.
- Boost_1 (en Boost_2) zijn nu zichtbaar op de US en via "Image Blending" → "Image Blending" is het mogelijk om tussen US-pre en T2 heen en weer te gaan
- Volg Boost_1 V_{150} gedurende de procedure en probeer hier een zo hoog mogelijke waarde te krijgen zonder de andere structuren te veel dosis te geven
- Bekijk de dosimetrie van Boost_2 in het tabblad "DVH"
- *Ga verder met de procedure zoals gebruikelijk*
- ...
- *Na de registratie van US-post en de CBCT*
- Registeer de CBCT met de MRI studie via "Image Fusion" → "Import Image Volume"
- Noem het nieuwe volume "mri" en klik "OK"
- Kies "MRI" als secondary structure en klik "OK"
- Klik "Register"
- Voer de registratie op basis van de FMs uit en, indien nodig, pas de registratie handmatig aan d.m.v. translatie en/of rotatie
- Vergelijk de prostaat contouren van de CBCT met de contouren van de MRI
- Klik "OK" om de uiteindelijke registratie te accepteren
- Importeer Boost_1 (en Boost_2) door de structuur te slecteren en op het pijltje te klikken

- Contoleer of de boost volumes binnen te prostaat liggen en niet afgeknipt werden door de registratie. Pas de contour desnoods aan.
- Boost_1 (en Boost_2) zijn nu zichtbaar op de CBCT (en US-post) en via "Image Fusion" $\rightarrow$ "Image Blending" is het mogelijk om tussen US-post, CBCT en T2 heen en weer te gaan
- Check de dosimetrie van Boost_1 en Boost_2 in het tabblad "DVH"
- *Ga verder met de procedure zoals gebruikelijk*